Geophys. J. R. astr. Soc. (1975) **43**, 453–499.

The Crust and Upper Mantle of Central Mexico

James E. Fix

(Received 1975 February 21)*

Summary

Six strain and inertial seismographs at Queen Creek, Arizona (QC–AZ), recorded six modes of surface waves from a suite of 18 earthquakes near Chiapas, Mexico. The six group-velocity dispersion curves were used in a least-squares inversion to estimate the shear velocity structure of the upper 380 km of crust and mantle in central Mexico. Multiple filter analysis of 108 seismograms produced group velocity dispersion curves slower than average continental paths. The range of the average deviation from the mean dispersion curve for the fundamental modes was 0·025 to 0·160 km s^{-1} for Rayleigh waves and 0·025–0·281 km s^{-1} for Love waves. The inversion models have low velocities that correspond with a representative geotherm and petrologic P–T diagrams to indicate partial melting. The 4-layer crust is 30 km thick with a high-temperature gradient LVZ in the granitic layer and with a LVZ in the lower 8 km of a basaltic layer resulting from a high geothermal gradient or from partial melting of water saturated rock. The mantle has a 4–8 km thick solid lid and a shallow low velocity zone. The lowest velocities correspond to 10–20 per cent partial melting. A sharp velocity gradient at 70–80 km probably results from both the phase change to garnet pyrolite and the lower extreme of partial water pressure with the disappearance of amphiboles from the host pyrolite. Based on the velocities, 5 per cent anhydrous melting extends to 260 km. From 300 to 380 km temperature gradients and crystal lattice instabilities prior to the olivine–spinel phase change produce another LVZ. A hypothesis is presented that the large volume of low density magma produces a regional vertical force that creates high flat plateaus as found in central Mexico and the Colorado Plateau. The inversion models have a 7·5 s S-wave residual relative to the Canadian Shield model CANSD in agreement with observed US station anomalies.

Introduction

The properties of the whole Earth are becoming well known through the inversion of combinations of body wave travel times and of various sets of the free oscillation frequencies in conjunction with the mass of the Earth and the moment of inertia of the Earth. As the gross properties of an average earth are better established, the variations from this average become more apparent and convincing.

This paper looks at the structure of the upper 380 km of the Earth in a region of major variation from the average. The shear-wave structure of the crust and upper

* Received in original form 1974 August 19

Table 1

Hypocentral data for earthquakes near the coast of Chiapas, Mexico, from Preliminary Determination of Epicentres and International Seismological Centre

Event	Date	Time GCT	N. latitude	W. longitude	Depth (km)	m_b	Azimuth station to epicentre	Distance deg	Distance km	Data source
1	1970 April 29	1122:36·4	14·618	92·690	41	5·6	132·5	25·2	2307·6	PDE
		1122:35·8±0·71	14·55±0·043	92·75±0·038	36±6·3	5·4	132·8	25·3	2809·5	ISC
2	1970 April 29	1207:30·7	14·231	92·811	33	5·1	133·3	25·5	2832·8	PDE
		1207:27±5·1	14·2±0·12	92·69±0·064	7±28	5·0	133·2	25·6	2843·5	ISC
3	1970 April 29	1229:19·3	14·527	92·645	33	4·5	132·6	25·3	2818·4	PDE
		1229:41±1·0	14·93±0·080	92·83±0·053	218±7·3	4·3	132·3	24·9	2771·6	ISC
4	1970 April 29	1252:52·6	14·457	92·778	33	4·5	132·9	25·3	2815·2	PDE
		1252:52±2·2	14·1±0·17	92·93±0·074	43±11	4·5	133·7	25·5	2835·9	ISC
5	1970 April 29	1929:52·3	14·671	93·499	29	5·2	133·9	24·7	2748·4	PDE
		1929:54·8±0·60	14·83±0·045	93·48±0·039	40±5·2	5·2	133·6	24·6	2735·8	ISC
6	1970 April 29	1938:32·3	14·561	93·552	33	4·9	134·2	24·8	2754·3	PDE
		1938:33±1·1	14·56±0·086	93·63±0·050	37±6·8	4·8	134·3	24·7	2749·1	ISC
7	1970 April 29	2033:39·9	14·317	92·686	33	4·9	133·0	25·5	2833·5	PDE
		2033:42·5±0·45	14·40±0·035	92·69±0·030	50±4·1	4·9	132·9	25·4	2826·4	ISC
8	1970 April 29	2047:47·3	14·446	92·866	33	4·6	133·1	25·3	2810·1	PDE
		2047:50±1·6	14·5±0·14	92·91±0·051	49±8·0	4·6	133·1	25·2	2802·8	ISC
9	1970 April 30	0043	not listed							PDE
		0043:26±2·9	14·7±0·10	92·71±0·074	25±20	4·1	132·5	25·2	2799·4	ISC

Table 1 (*continued*)

10	1970 April 30	0054:13·6	14·457	93·050	57	4·9	133·4	25·2	2796·7	PDE
		0054:14·6±0·80	14·51±0·063	93·09±0·053	61±7·4	4·8	133·4	25·1	2789·7	ISC
11	1970 April 30	0358:24·3	14·506	93·170	33	4·5	133·6	25·0	2784·3	PDE
		0358:28·8±0·85	14:65±0·087	93·07±0·055	70±6·5	4·3	133·2	25·0	2779·1	ISC
12	1970 April 30	0359:50·2	14·662	93·044	33	5·1	133·1	25·0	2780·0	PDE
		0359:54·6±0·86	14·67±0·049	93·03±0·052	71±7·9	4·9	133·1	25·0	2780·1	ISC
13	1970 April 30	0546:22·0	14·431	93·330	33	4·9	134·0	25·0	2780·4	PDE
		0546:24·7±0·60	14·56±0·044	93·31±0·038	48±5·2	4·9	133·7	24·9	2770·6	ISC
14	1970 April 30	0832:59·1	14·698	93·192	19	5·6	133·3	24·9	2766·5	PDE
		0833:01·1±0·69	14·61±0·034	93·29±0·031	37±6·1	5·8	133·6	24·9	2767·6	ISC
15	1970 April 30	0859:07·6	14·531	93·400	33	5·2	133·9	24·9	2767·1	PDE
		0859:08±1·1	14·56±0·060	93·24±0·068	35±9·1	5·1	133·6	25·0	2775·3	ISC
16	1970 April 30	1251:36·3	14·447	93·430	24	5·3	134·1	24·9	2772·0	PDE
		1251:37±1·2	14·50±0·048	93·36±0·038	24±8·8	5·4	133·9	24·9	2772·4	ISC
17	1970 April 30	1321:03·2	14·476	93·498	22	5·4	134·2	24·9	2764·9	PDE
		1321:04±1·2	14·65±0·047	93·40±0·037	17±8·3	5·3	133·8	24·8	2756·7	ISC
18	1970 April 30	1545:12·4	13·955	92·873	33	4·5	133·8	25·6	2851·8	PDE
		1545:09±5·4	13·7±0·24	92·89±0·087	26±27	4·5	134·2	25·8	2873·2	ISC

Note

PDE depths given as 33 were listed as N and were constrained to 33 in the solution.

mantle of a path along the centre of Mexico from about 14 to 33 degrees north latitude is established by inversion of Rayleigh-wave and Love-wave group velocities for the fundamental modes, the first higher modes, and the second higher modes from 108 earthquake–instrument pairs.

Data

The data used in this study were surface waves from a suite of 18 closely-grouped earthquakes near the coast of Chiapas, Mexico, that were recorded at the Queen Creek Seismological Station (QC–AZ). QC–AZ is about 50 km south-east of Phoenix, Arizona. The instrumentation at QC–AZ consisted of 3-component high-sensitivity inertial and strain seismographs recorded in several passbands (Fix & Sherwin 1970). The surface waves recorded in the long-period (LP) passband on the three strain and three inertial seismographs were used in this study providing a possible 108 earthquake–instrument pairs.

The hypocentral data from the Preliminary Determination of Epicenters (PDE) lists of the National Ocean Survey (NOS) (the organizational name at that time) and from the International Seismological Center (ISC) lists are given in Table 1 along with calculated epicentral distances and azimuths from the station to the epicentres. The epicentral distances based on the two lists are in agreement within 0·1–20·7 km for all the earthquakes except number 3 for which the ISC solution had a depth of 218 km. This slight variation in epicentral locations is within the normal tolerance expected for routine locations. The differences in epicentral distances for each earthquake are all less than 1 per cent of the total distance and will result in less than a 1 per cent variation in observed group velocities based either on the PDE epicentre or on the ISC epicentre. The PDE data were the only set available at the beginning of the study and were used for the calculations leading to the observed group velocities.

The epicentral region, the location of QC–AZ, and the path between them are shown in Fig. 1.

The geologic structure of Mexico is a continuation of the general structure of the western United States (WUS). The structure parallels the Gulf of California–Pacific Ocean coast line. The Sierra Madre Occidental is a high mountain chain near the west coast. To the east of the Sierra Madre Occidental is a high plateau, the Mesa Central, that has an uplift and valley structure that resembles the Basin and Range. The Sierra Madre Oriental contains many folded belts on the east that grade into the Gulf of Mexico coastal plain. Between north latitudes of about 18–20 deg a line of volcanoes and recent volcanic activity extends from the Pacific Ocean to the Gulf of Mexico. To the south of the line of volcanoes is an extensive metamorphosed region (King 1969; de Cserna 1961).

The 3-component inertial seismograms from event 16 are illustrated in Fig. 2. (The LP seismometers have a natural period of 17·3 s. The galvanometers have a natural period of 110 s; and the system amplitude response peaks at 25 s.) These recordings are typical of the signals from all 18 earthquakes. The horizontal seismographs were oriented in azimuths of 325 deg and 55 deg to take advantage of the QC–AZ mine configuration. All 18 earthquakes were at azimuths of 132·3–134·2 deg from QZ–AZ. These azimuths are about 12 deg off the back azimuth of the 325 deg instruments providing essentially a radial and a transverse orientation of the horizontal seismographs. Because of this orientation and the separation of wave types on the seismograms, the group velocities were calculated from the seismograms as recorded. The *P*-wave arrival is seen on the PZLL vertical seismogram and on the radial P325LL horizontal seismogram, but not on the transverse P55LL horizontal seismogram. (Nomenclature: P = pendulum, Z = vertical, 325, 55 = azimuth for up on recording, first L = LP response, second L = low gain channel). The *SH* arrival

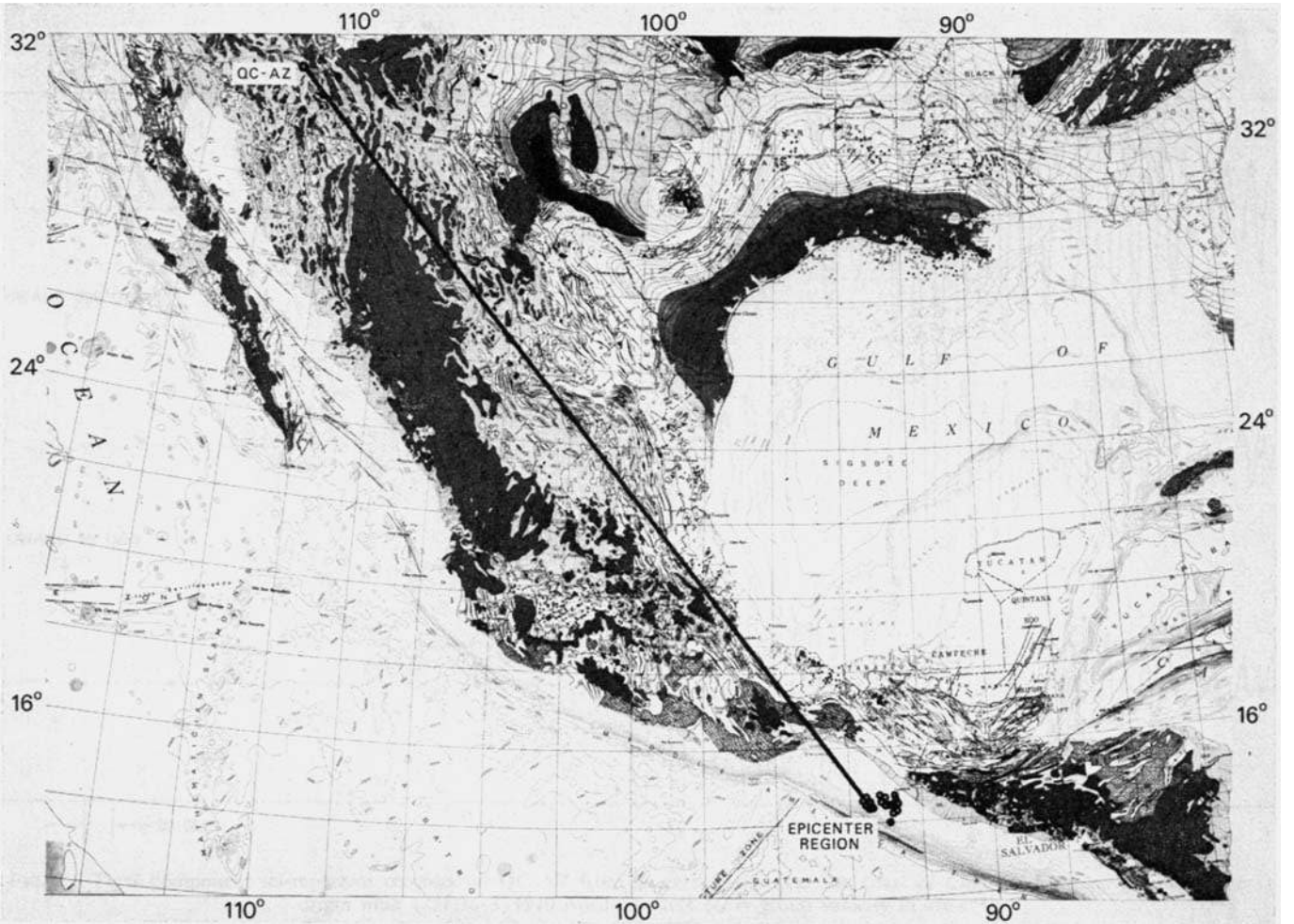

FIG. 1. Map showing the epicentral region, the location of QC–AZ, and the great circle path between them. Base map from Tectonic Map of North America (King 1969).

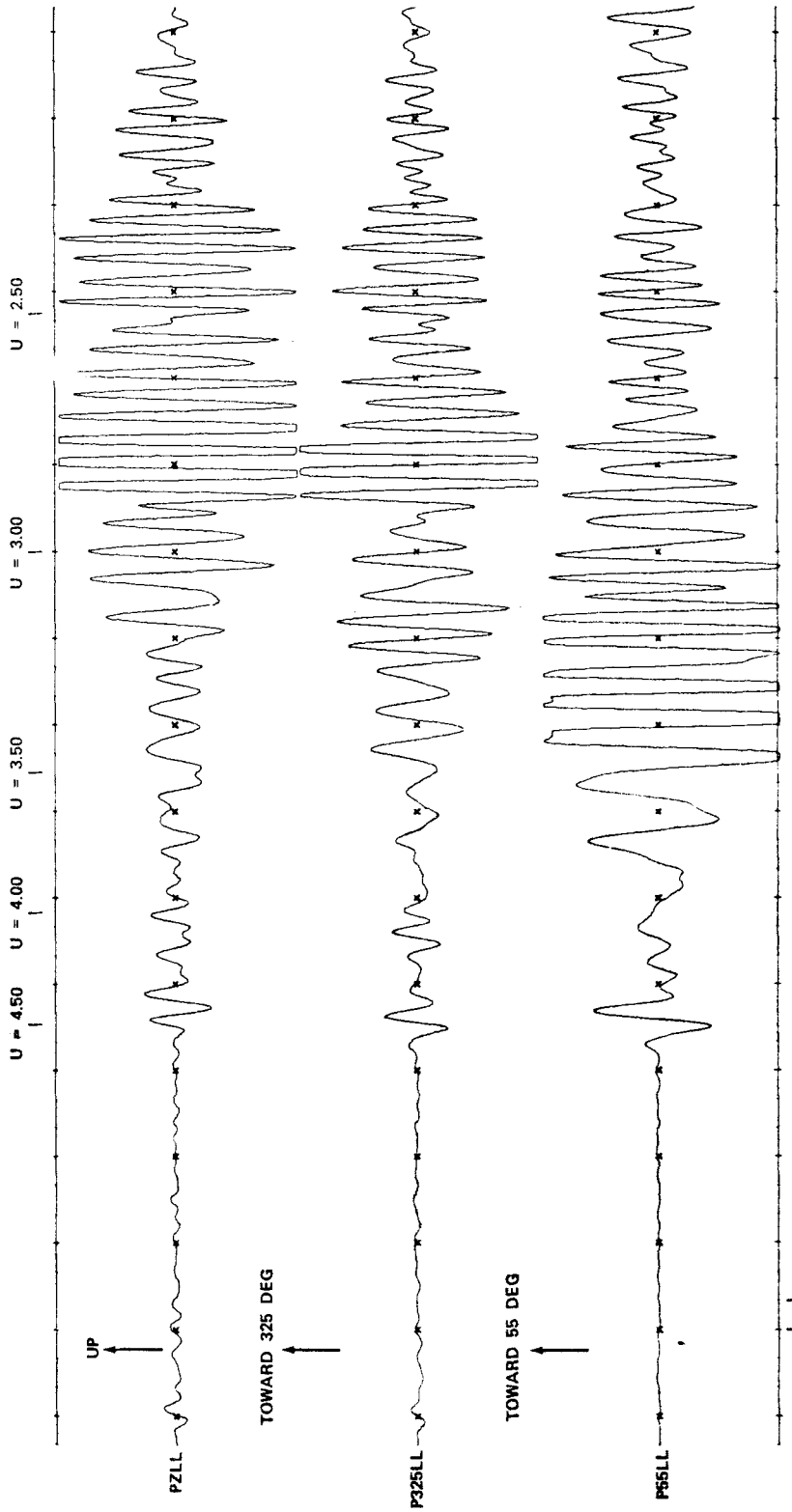

FIG. 2. Three-component seismograms recorded at QC–AZ from an earthquake near the coast of Chiapas, Mexico. Event number 16, origin time 1251:36·3, 1970 April 30, GCT (U = group velocity in km s^{-1}).

is very distinct on the P55LL transverse trace and the *SV* arrival about 10 s later is distinct on the PZLL. The *S* arrival on the P325LL trace appears to be a mixture of *SH* and *SV* motion. The Love-wave fundamental mode and higher modes are recorded on the P55LL seismogram. The Rayleigh-wave fundamental mode and higher modes are recorded on the PZLL and P325LL seismograms. A small amount of Love-wave energy can be seen in the P325LL seismogram. Both the Rayleigh-wave train and the Love-wave train contain a beat at a group velocity of about 2·5 km s^{-1}. This beat and the following signals are interpreted as a multipath effect from a lateral refraction. A few of the peaks are clipped on each of the seismograms where the signal exceeded the maximum amplitude on the magnetic tape recorder low gain channels.

Method

The method used to obtain the shear wave velocity structure is similar to that of other investigators. The observed group velocities were obtained. A starting model was established. Partial derivatives of group velocity relative to shear wave velocity were calculated for the various layers of the model. Then, a least squares inversion was performed to obtain the shear wave velocity structure. Each of the aspects of the method is discussed in the following paragraphs.

The observed group velocities were obtained by the 'multiple filter technique' (Dziewonski, Bloch & Landisman 1969). In the multiple filter technique, the digitized seismic signals are transformed to the frequency domain with the Fast Fourier Transform (FFT), the frequency coefficients are passed through a group of narrow-band Gaussian filters centred at selected frequencies, a quadrature spectrum is formed, filtered in-phase and quadrature spectra are transformed with the FFT to the time domain to form the envelope of the filtered traces at the selected frequencies (Bracewell 1965), the instantaneous amplitude and phase are established at the specified group velocities, the amplitudes are normalized to a maximum value of 99 based on both a linear normalization and a decibel (dB) normalization, and the results are printed as a function of group velocity and logarithm of the period. The amplitudes are manually contoured to aid in selection of the maxima which define the dispersion curves. Herrmann (1973) has shown that with the Gaussian filter, if the spectral amplitude of the signal is not a function of frequency within the narrow-band limits of the filter, the instantaneous amplitude is a maximum at a time $t = r/U_0$ where r is the epicentral distance and U_0 is the group velocity at angular frequency ω_0. He has also shown that the Gaussian filter suppresses the dependence of the amplitude estimate upon the epicentral distance and the shape of the group velocity curve. Herrmann defined a time duration t_d for the Gaussian time domain envelope to decay from the peak value to an amplitude of exp $(-\pi)$. In terms of the period of the signal T_0 and α, a parameter of the filter

$$t_d = T_0 \sqrt{\frac{\alpha}{\pi}}. \tag{1}$$

He concluded that if two maxima are separated by a time greater than $2t_d$, then two modes are not interfering and group velocities can be unambiguously established. In the Gaussian filters used in this work, α equals 36·9. This value was selected for α for a time-bandwidth product that provided a compromise between resolution in the time domain and in the frequency domain (Dziewonski *et al.* 1969; Papoulis 1962). The resulting time durations t_d are 3·4 T_0.

The multiple filter technique was applied to the 108 seismograms over the two decade period range from 2·90 to 290·7 s with 83 periods and over the group velocity window from 5·00 to 1·00 km s^{-1} at 0·02 km s^{-1} intervals. The printed amplitudes

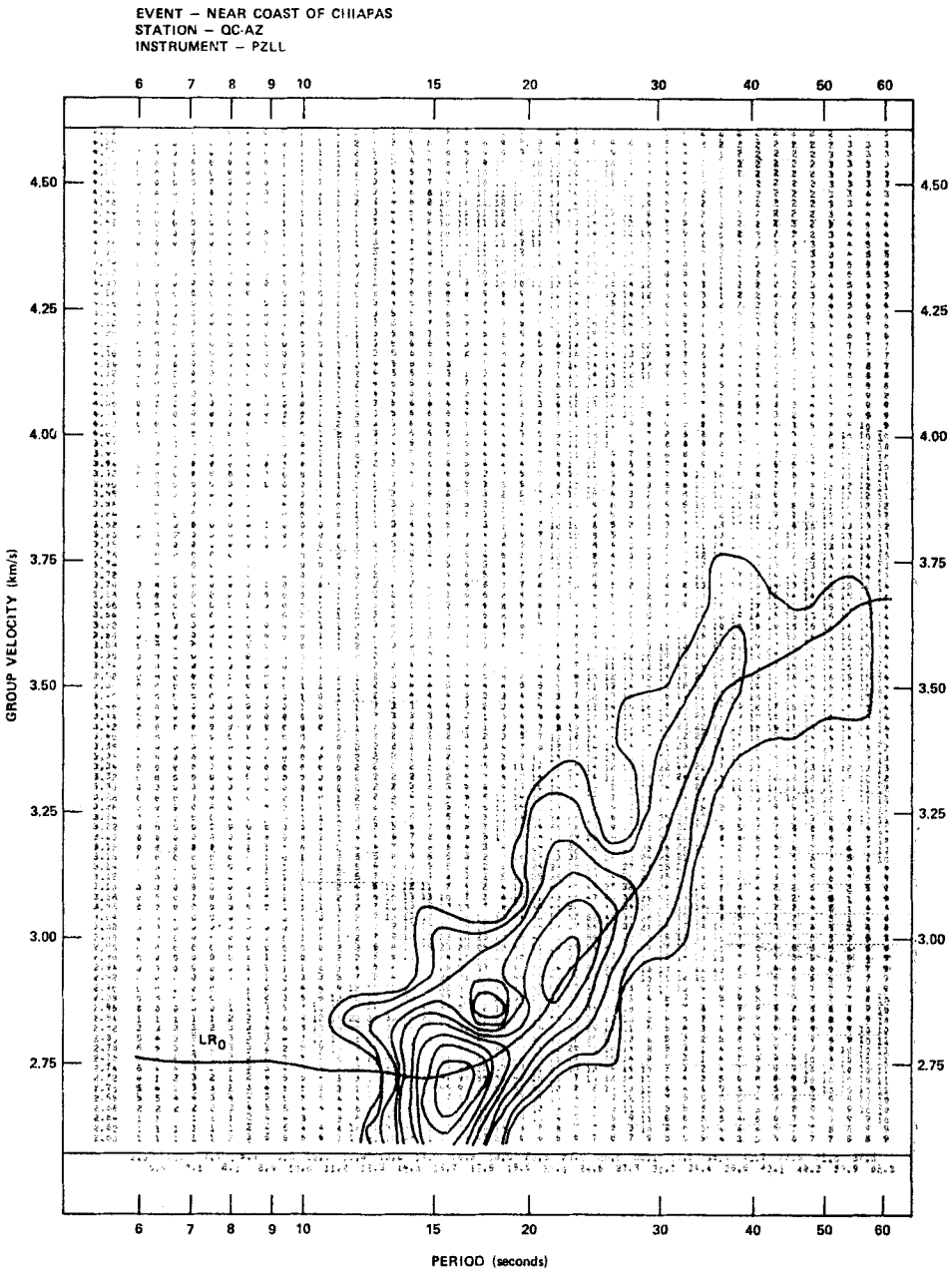

FIG. 3. Multiple filter analysis of surface waves from an earthquake near the coast of Chiapas, Mexico, 1970 April 30, 1251:36·3 origin time, recorded on vertical inertial seismograph PZLL.

were contoured and the dispersion curves were drawn for each of the earthquake–instrument pairs. Examples of the multiple filter analysis technique applied to event number 16, 1970 April 30, 1251 : 36·3 origin time, are given in Fig. 3 for the vertical inertial seismograph PZLL, in Fig. 4 for the radial horizontal seismograph P325LL, and in Fig. 5 for the transverse horizontal seismograph P55LL. The curves plotted in

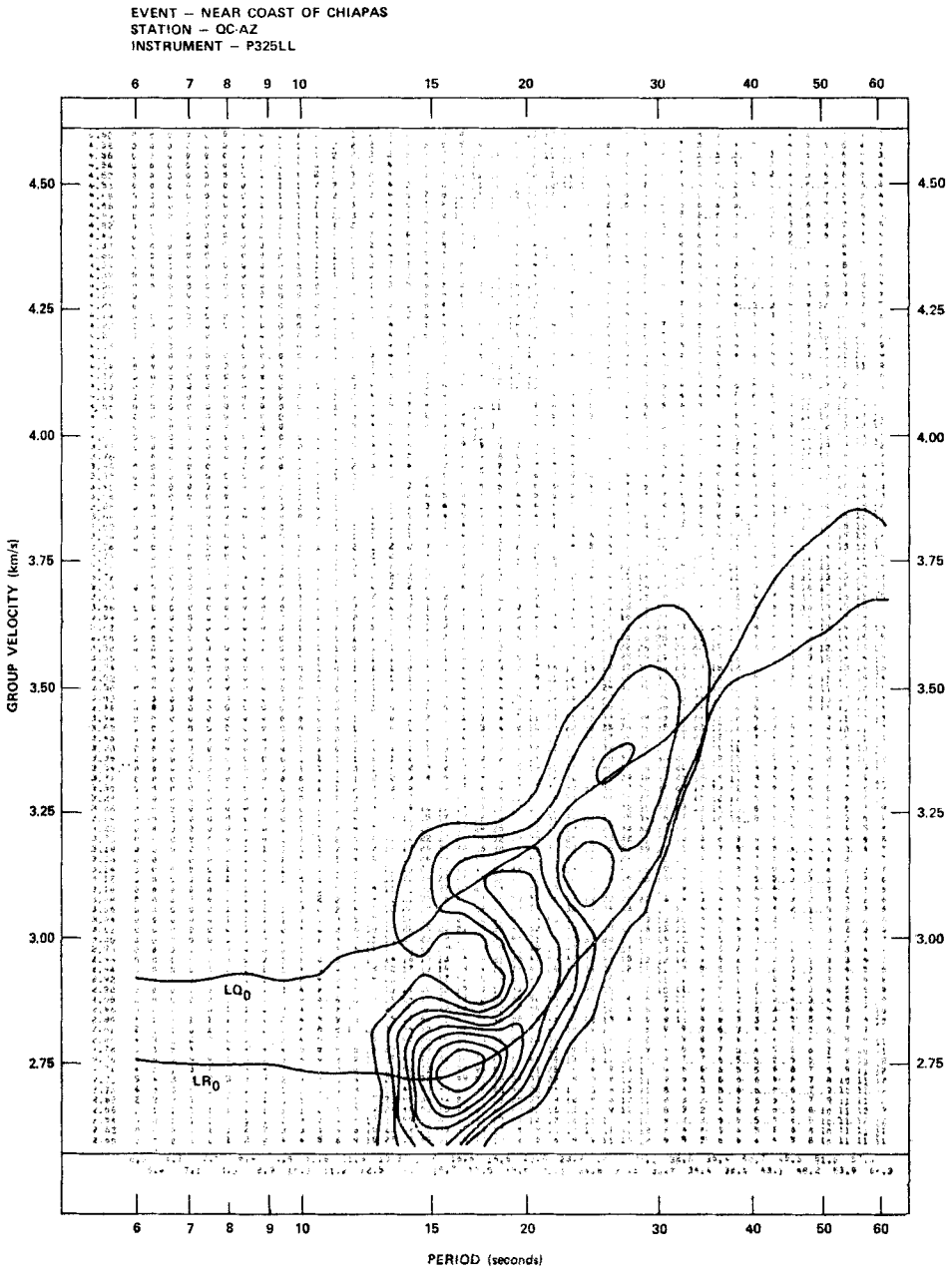

FIG. 4. Multiple filter analysis of surface waves from an earthquake near the coast of Chiapas, Mexico, 1970 April 30, 1251:36·3 origin time, recorded on radial inertial seismograph P325LL.

the figures are the smoothed mean group-velocity dispersion curves; they will be discussed later. Despite the fact that the horizontal seismographs are only 12 deg off radial and transverse orientation, some signals from the non-wanted mode appear in the analysis. These signals are not evident in the seismograms (Fig. 2). The fundamental Rayleigh-wave (LR_0) dispersion curve and the fundamental Love-wave

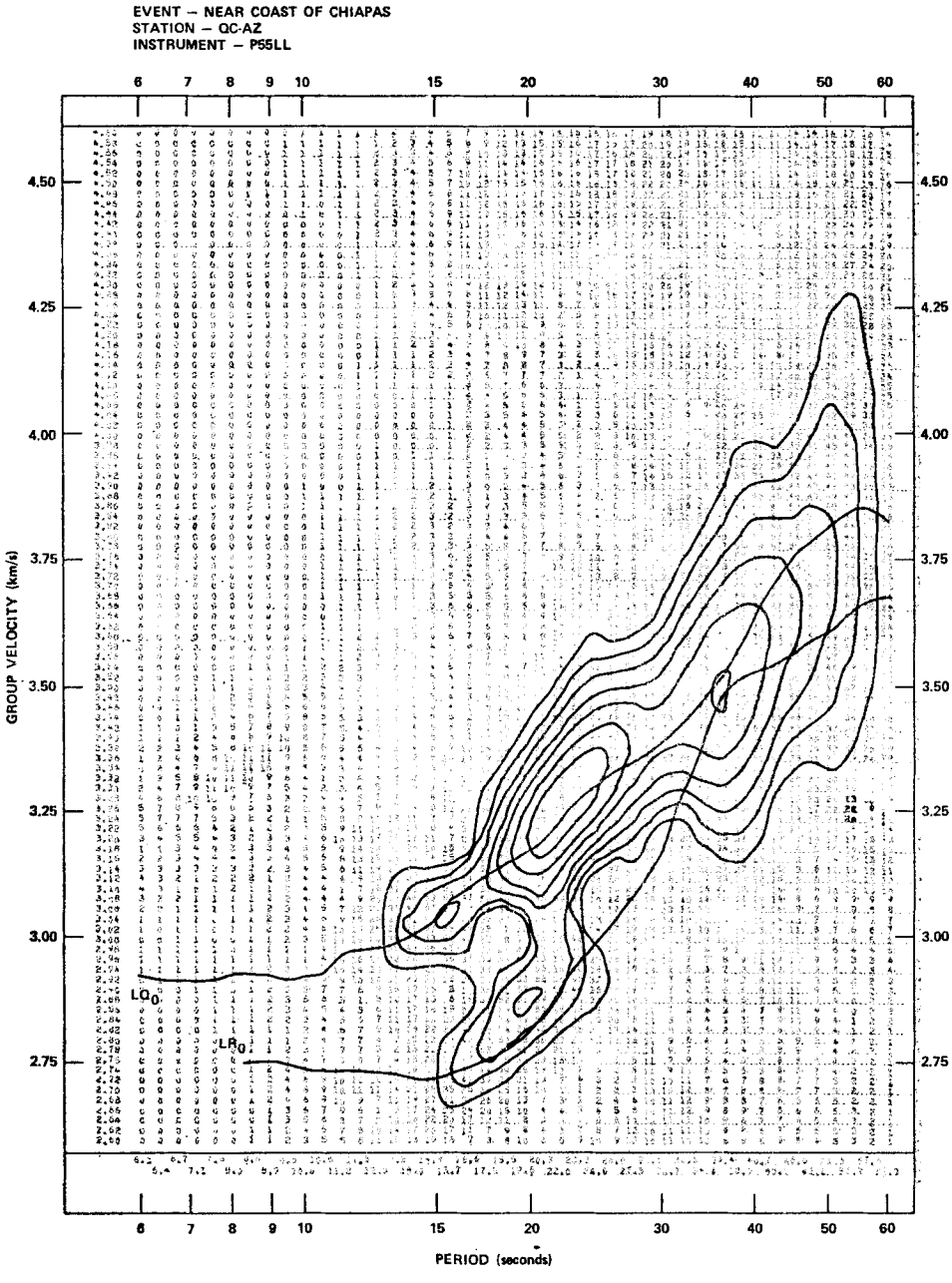

FIG. 5. Multiple filter analysis of surface waves from an earthquake near the coast of Chiapas, Mexico, 1970 April 30, 1251:36·3 origin time, recorded on transverse inertial seismograph P55LL.

(LQ_0) dispersion curve approach each other at periods between 35 and 40 s. However, with the multiple filter analysis, the dispersion curve is well established on both sides of this region and can be satisfactorily continued through it. The group velocities of the amplitude maxima were tabulated for the periods of the analysis. The sample mean, median, standard deviation (second moment), and average deviation from the

mean (first moment) were calculated from the data set for each mode. The sample mean group velocities were smoothed with a seven-point least squares smoothing function (Lanczos 1956). The smoothed sample means were used in the inversion process.

The initial phase and geometric orientation of a source of Rayleigh waves can affect the apparent group velocity. Knopoff & Schwab (1968) derived an expression for the group velocity U of

$$U = \frac{r}{t - (d\Psi/d\omega)} \tag{2}$$

where r is epicentral distance, t is time, Ψ is a phase angle determined from the source parameters, and ω is angular frequency. Empirically, they found that for a point source dipping 45 deg away from the detector and for two structure models (2) could be approximated by

$$\frac{1}{U} = \frac{1}{\bar{U}} - \frac{2{\cdot}073}{r} \tag{3}$$

where $\bar{U}$ is the group velocity for a vertical or horizontal source. One structure model was a simple layered crust over a semi-infinite half-space and the other structure model was derived for the crust and upper mantle north of the Alpine crest and contained an S-wave low-velocity channel. Equation (3) implies a shift in origin time of 2·073 s for the models and source considered by Knopoff & Schwab (1968). The earthquakes used in this study were at epicentral distances of about 2800 km (Table 1). It was assumed that the effect of the initial phase of the source was comparable to or less than that of the Alpine model of Knopoff & Schwab. Since 2·8 s is 0·1 per cent of the total travel time, the effect of the initial phase was neglected in this study.

The initial model for the inversion process was established from the models of previous investigators. The P-wave velocity models considered were from a central Mexico non-reversed refraction profile of the Carnegie Institute of Terrestrial Magnetism (Steinhart & Meyer 1961; Press 1966), an extensive refraction survey in the vicinity of the Tonto Forest Observatory (TFO) by Warren (1969), an inversion of the ray parameter $p = dT/d\Delta$ determined from an extended TFO array by Johnson (1967), and Basin and Range P-wave travel-time inversions by Green & Hales (1968), Archambeau, Flinn & Lambert (1969), Massé (1971), Massé, Landisman & Jenkins (1972), and Wiggins & Helmberger (1973). The S-wave velocity models considered (see Fig. 6) were from trial and error fits to Love-wave phase velocities between Dugway and Tucson by Wickens & Pec (1968) and to Basin and Range Rayleigh-wave phase velocities by Pilant (1967), S-wave travel-time inversions by Lehmann (1955; Dorman, Ewing & Oliver 1960), Ibrahim & Nuttli (1967), Nuttli (1969), and Hales & Roberts (1970), and an inversion of S-wave $dT/d\Delta$ from the TFO extended array by Kovach & Robinson (1969). The initial model FBR1 was taken from (a) two upper crustal layer P velocities from Warren (1969), (b) top layer, lower crust, and mantle P velocities from Massé (1971; Massé *et al.* 1972), (c) S velocities for the mantle and the third crustal layer from Kovach & Robinson (1969), (d) the S velocity of the top layer was obtained from Massé's P velocity and an assumed Poisson ratio of 0·33, (e) the S velocity of the second layer was obtained from Warren's P velocity and the Poisson ratio of 0·321 determined by Fix for QC–AZ (Fix & Sherwin 1972), (f) the depth of the interfaces and the division of the model into discrete layers was a minor compromise between the models of Massé and Kovach and Robinson with a requirement that both P-wave and S-wave interfaces be at the same depths, and (g) the densities were taken from the Nafe and Drake (Talwani, Sutton & Worzel 1959; Press 1966) empirical relation between P-wave velocity and density. Theoretical dispersion curves were calculated for the initial model, but they did not resemble the

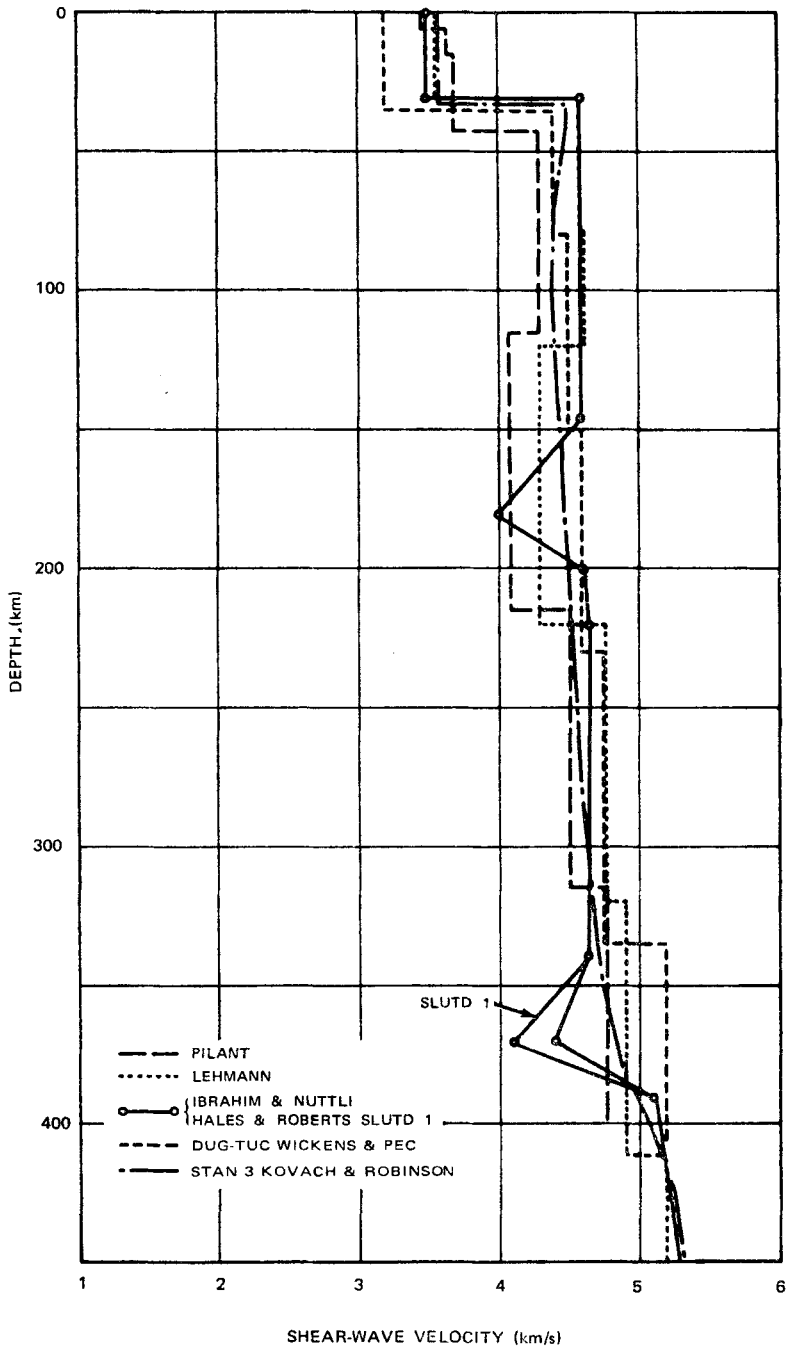

FIG. 6. Shear-wave velocity models from the literature.

finer points of the observed dispersion curves. Therefore, three other models were constructed using seismic velocities calculated by Birch (1969) for spherical partial melt nodules in olivine plus a basaltic melt along the solidus. One model had the original *P*-velocity structure and an *S*-wave structure with no lid and 5 per cent melt.

The other two models had *P*-wave and *S*-wave structures representing 10 per cent melt; one model had a lid and the other model did not. The model with a 16 km thick lid and 10 per cent melt was adopted as the starting model FBR3 because the group velocities had a maximum at about 45 s and a minimum at about 90 s. The starting model FBR3 is given in Table 2 and the shear-wave velocities are plotted with the inversion models. During the course of the study, some instabilities were experienced with inversions using the relatively thin layers of model FBR3. An abbreviated form of the model (FBR3A) was created with fewer, thicker layers. Model FBR3A, given in Table 3, has essentially the same structure as model FBR3.

Table 2

Starting model FBR3

Layer No.	Depth (at bottom of layer) (km)	Thickness (km)	Compressional wave velocity (km s^{-1})	Shear wave velocity (km s^{-1})	Density (g cm^{-3})
1	1	1	3·000	1·500	2·32
2	2	1	5·590	2·87	2·62
3	4	2	5·590	2·87	2·62
4	6	2	6·12	3·58	2·90
5	10	4	6·12	3·58	2·90
6	14	4	6·12	3·58	2·90
7	18	4	6·12	3·58	2·90
8	22	4	6·91	3·80	3·09
9	26	4	6·91	3·80	3·09
10	30	4	6·91	3·80	3·09
11	34	4	7·49	4·50	3·26
12	38	4	7·49	4·50	3·26
13	42	4	7·80	4·50	3·32
14	46	4	7·80	4·50	3·32
15	50	4	7·75	4·47	3·31
16	60	10	7·60	4·33	3·30
17	70	10	7·37	4·12	3·30
18	80	10	7·38	4·12	3·30
19	100	20	7·40	4·13	3·30
20	120	20	7·42	4·14	3·30
21	140	20	7·49	4·16	3·30
22	150	10	7·45	4·17	3·39
23	160	10	7·76	4·28	3·45
24	180	20	8·350	4·489	3·50
25	200	20	8·350	4·504	3·50
26	220	20	8·380	4·609	3·51
27	240	20	8·380	4·609	3·51
28	260	20	8·380	4·609	3·51
29	280	20	8·380	4·609	3·51
30	300	20	8·600	4·609	3·55
31	320	20	8·800	4·706	3·62
32	340	20	8·80	4·740	3·62
33	360	20	9·01	4·82	3·69
34	380	20	9·25	4·89	3·75
35	400	20	9·25	5·07	3·90
36	420	20	9·625	5·250	4·01
37	460	40	9·650	5·320	4·06
38	500	40	9·67	5·38	4·11
39	550	50	9·70	5·44	4·15
40	600	50	9·80	5·51	4·23
41	625	25	9·90	5·57	4·26
42	645	20	10·85	5·90	4·51
43	700	55	10·95	6·14	4·69
44	½ space	∞	10·95	6·14	4·69

Table 3

Starting model FBR3A

Layer No.	Depth (at bottom of layer) km	Thickness km	Compressional wave velocity km s^{-1}	Shear wave velocity km s^{-1}	Density g cm^{-3}
1	1	1	3·00	1·50	2·32
2	4	3	5·59	2·87	2·62
3	18	14	6·12	3·58	2·90
4	30	12	6·91	3·80	3·09
5	38	8	7·49	4·50	3·26
6	50	12	7·80	4·50	3·32
7	80	30	7·37	4·12	3·30
8	120	40	7·42	4·14	3·30
9	160	40	7·45	4·17	3·39
10	200	40	8·35	4·50	3·50
11	260	60	8·38	4·609	3·51
12	300	40	8·60	4·609	3·55
13	340	40	8·80	4·72	3·62
14	380	40	9·25	4·89	3·75
15	420	40	9·625	5·07	3·90
16	460	40	9·65	5·32	4·06
17	500	40	9·67	5·38	4·11
18	½ space	∞	9·70	5·44	4·15

Theoretical phase velocity and group velocity dispersion curves were calculated for the fundamental and the first five higher modes of Rayleigh waves and Love waves. The theoretical calculations were made with a computer program originally written by Dorman (Dorman *et al.* 1960) modified by Robert P. Massé and again modified by the present author. The program uses the Thompson–Haskell matrix method (Thompson 1950; Haskell 1953; Harkrider 1964) with matrix factoring for Rayleigh waves as suggested by Dunkin (1965) to minimize numerical problems at the shorter wave lengths. The program contains an option to correct the flat earth model to equivalent spherical earth properties. The Rayleigh-wave correction is only an approximation (Alterman, Jarosch & Pekeris 1961). The Love-wave correction is exact (Biswas & Knopoff 1970) and involves a change in the flat earth layer thicknesses, S velocities, and densities. Partial derivatives of group velocity with respect to layer shear velocity were calculated for each layer of models FBR3 and FBR3A for the several modes over a range of periods. The partial derivatives were calculated with a program written by the present author. This program perturbs the layer shear velocity by a small increment and calculates the partial derivative from the original group velocity, the perturbed group velocity, and the shear velocity increment. Harkrider (1968) has developed equations for Love-wave group velocity partial derivatives in terms of energy integrals based on variational principles. Since a computer program was not available to calculate the Love-wave partial derivatives from the energy integrals, and since Rayleigh-wave partial derivatives would have to be calculated numerically, all of the partial derivatives were obtained numerically by the same program. The partial derivatives of group velocity with respect to layer shear-wave velocity for the fundamental Rayleigh-wave mode and the fundamental Love-wave mode for model FBR3 are plotted in Figs 7 and 8 and for model FBR3A in Figs 9 and 10. There are several features of the partial derivatives that are significant to this study. For most mode-layer combinations, the partial derivatives are positive for some periods (generally the longer periods) and negative for other periods (generally the shorter periods). Thus, for any given mode and layer, information at one period can be cancelled, reinforced, or changed by information at another period.

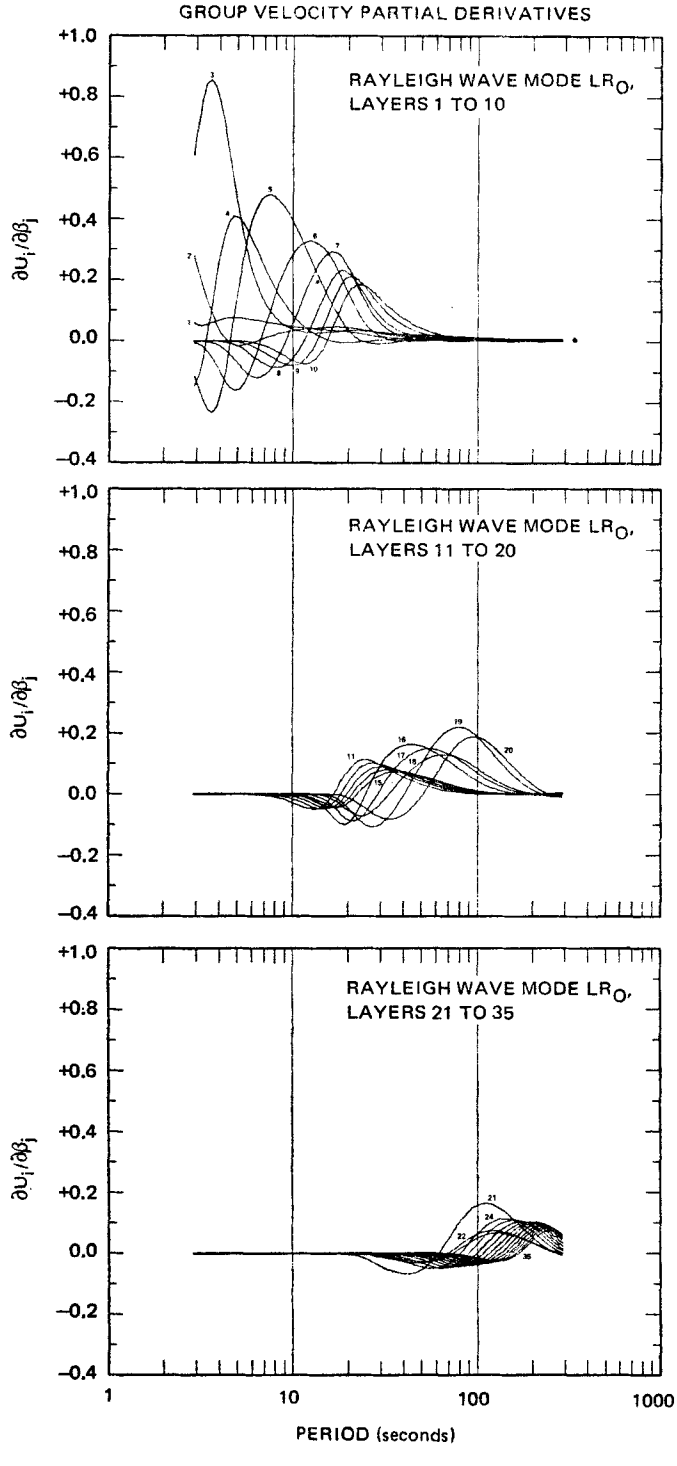

FIG. 7. Partial derivatives of fundamental Rayleigh-wave group velocity with respect to layer shear velocity for model FBR3.

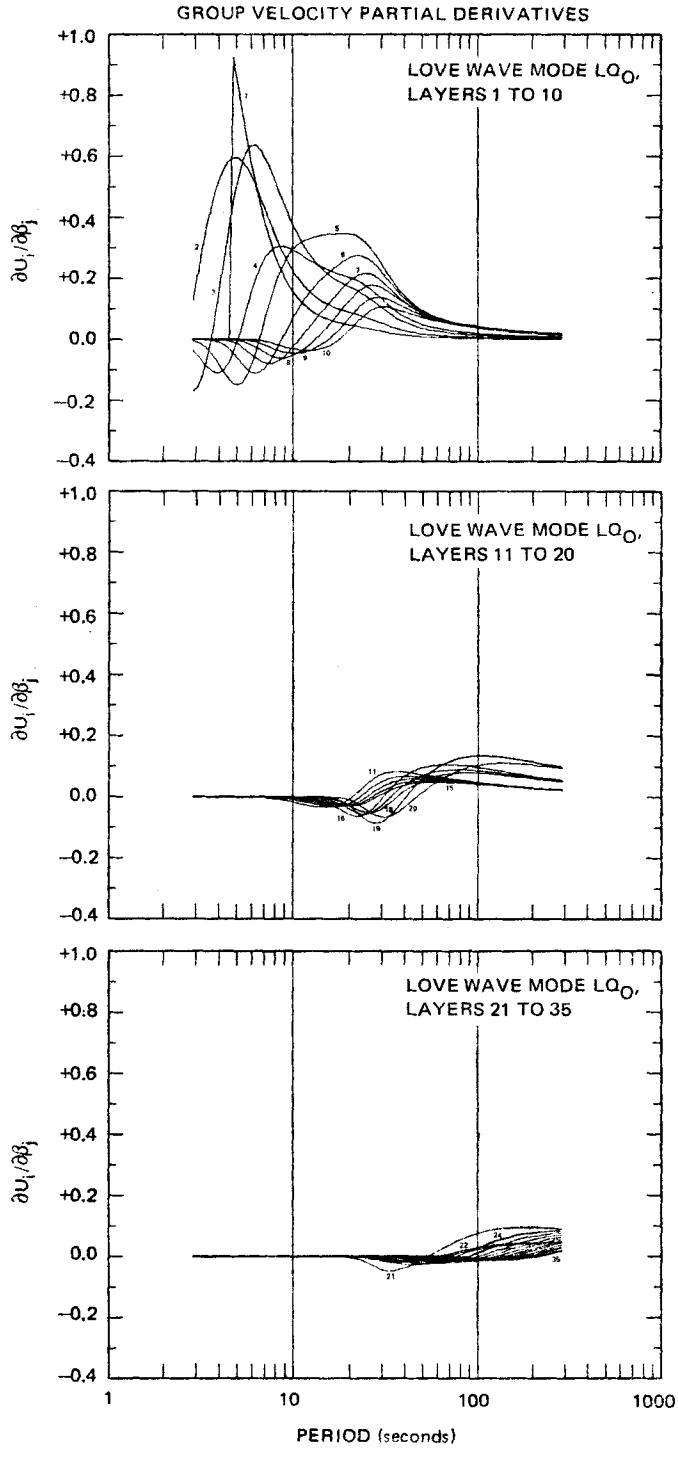

FIG. 8. Partial derivatives of fundamental Love-wave group velocity with respect to layer shear velocity for model FBR3.

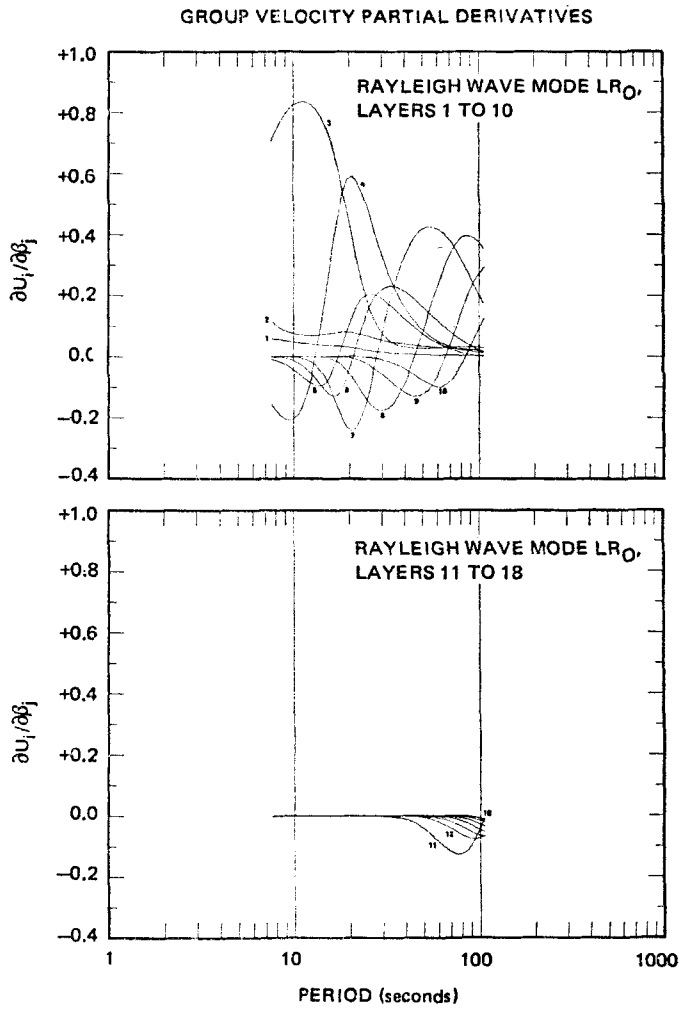

FIG. 9. Partial derivatives of fundamental Rayleigh-wave group velocity with respect to layer shear velocity for model FBR3A.

For most mode-period combinations, the partial derivatives for some layers are positive and for other layers, are negative. Thus, for any given mode and period, information relating to one layer can be cancelled, reinforced, or changed by the relationship among layers. In this manner, the partial derivative curves contain information relating to the resolution capability of an inversion process. The curves can be read as plotted to determine what periods most affect a given layer; or they can be read vertically to determine what layers are most affected at a given period.

Model FBR3 has thinner layers than model FBR3A and the partial derivatives have sharper peaks and overlap each other considerably more than the partial derivatives corresponding to the same depths for model FBR3A. The sharper peaks indicate better resolution, but the increased overlap presents problems of inversion instability and probably decreases the linear independence of information at adjacent periods. The majority of higher mode curves have large partial derivatives where the theoretical group-velocity dispersion curve changes rapidly between 3·5 and 4·0 s and between 6 and 8 s. These period ranges were avoided in the inversions. The Love-wave partial

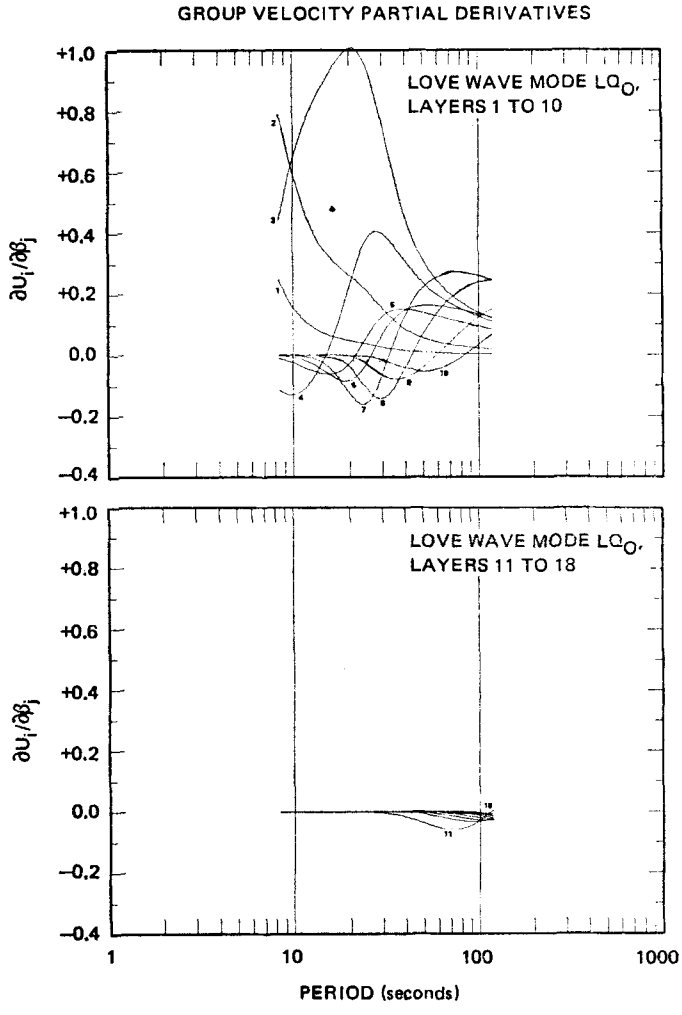

FIG. 10. Partial derivatives of fundamental mode Love-wave group velocity with respect to layer shear velocity for model FBR3A.

derivatives have broader peaks than the Rayleigh-wave partial derivatives. The Love-waves are more sensitive to the shallower structure and, at a given period, the Rayleigh-wave sensitivity extends to deeper depths than the Love-wave sensitivity. The partial derivatives for the layers in the low velocity zone (LVZ) are larger than the partial derivatives for the adjacent layers.

The inversion method used in this study is a least squares technique patterned after that developed and used by Bloch (1969; Bloch, Hales & Landisman 1969) and used by James (1971b). Bloch used phase velocities and group velocities for several modes to obtain the shear-wave velocity structure in southern Africa. James used trial and error inversion with phase velocities and Bloch's method of inversion with group velocities to obtain the shear-wave velocity structure in the Andes. To improve stability, the least squares process is applied to the shear velocity in one layer at a time proceeding through the set of layers included in the solution in a specified order. The process is then repeated for a selected number of iterations. The least-squares

numerical inversion of seismic surface wave phase velocity dispersion data to obtain properties of the crust and mantle was first utilized by Dorman & Ewing (1962) in the New York–Pennsylvania area. Brune & Dorman (1963) applied this method to phase velocities of surface waves propagated across the Canadian Shield. McEvilly (1964) used this technique to invert phase velocities to obtain a model of the crust and upper mantle in the central United States.

If a set of group velocities $U_{0_{mi}}$ are observed for given modes m at a set of periods T_{mi}, and if a set of theoretical group velocities $U_{T_{mi}}$ are calculated for the same modes and periods from a model, the least squares problem is to minimize the sum of the squares of the residuals R_{mi}
where

$$R_{mi} = U_{0_{mi}} - U_{T_{mi}} \qquad m = 1, 2, \ldots, \mathrm{NM} \qquad i = 1, 2, \ldots, \mathrm{IP}_m \tag{4}$$

and NM is the number of modes and IP_m is the number of periods for mode m. Thus, we want to minimize

$$\sum_{m=1}^{\mathrm{NM}} \sum_{i=1}^{\mathrm{IP}_m} \mathbf{R}_{mi}{}^2. \tag{5}$$

Assuming small changes and that there is a linear dependence between layer shear velocity and theoretical group velocity, and using the partial derivative of group velocity for mode m and period i with respect to shear-wave velocity β in layer $k = j$, we can write a set of equations

$$\frac{\partial U_{mi}}{\partial \beta_k} d\beta_j = \mathbf{R}_{mi} \tag{6}$$

or in matrix notation

$$\mathbf{PD} = \mathbf{R} \tag{7}$$

where $\mathbf{P}$ is a row vector of partial derivatives; $\mathbf{D}$ is a single element column vector of the change in shear velocity needed in layer $k = j$, and $\mathbf{R}$ is a column vector of residuals. If both sides are multiplied by the transpose of $\mathbf{P}$,

$$\mathbf{P}^T \mathbf{PD} = \mathbf{P}^T \mathbf{R}. \tag{8}$$

These equations are solved for $\mathbf{D}$ which is the least squares solution of (7) for the change in shear velocity $\Delta\beta$ of layer $k = j$. The theoretical group velocity is then revised by the set of equations

$$\Delta U_{T_{mi}} = \frac{\partial U_{mi}}{\partial \beta_k} \Delta\beta_j \tag{9}$$

$\mathbf{R}$ is revised by

$$\mathbf{R}_{mi}(\text{new}) = \mathbf{R}_{mi}(\text{old}) - \Delta U_{T_{mi}}. \tag{10}$$

The succeeding layers are each then treated in the same manner, until the change in all layers to be used in the solution has been calculated. The overall solution is then improved by repeating the entire process for several iterations.

The preceding discussion considered only group velocities and layer shear velocities. Other independent parameters such as phase velocities and Rayleigh-wave ellipticity (Boore & Toksöz 1969) could have been used separately or in combination with the other two parameters. Also other properties of the layers such as compressional wave velocity and density could be used, again separately or in combination. Dorman & Ewing (1962), Brune & Dorman (1963) and McEvilly (1964) used only phase velocities in their inversions. Bloch (1969; Bloch *et al.* 1969) used both phase velocities and group velocities. He came to the conclusion that the inversion of the group-velocity dispersion curve should produce a more detailed earth model than the inversion of the phase-velocity dispersion curve. This conclusion is based on the fact

that the group velocity is a derivative of the phase velocity and will have large variations for a corresponding small variation in the phase velocity. Knopoff (1972) and Pilant & Knopoff (1970) reason that inversion of phase velocities eliminates one degree of non-uniqueness present in the inversion of group velocities, because a single group velocity curve could fit several phase velocity curves that were displaced from each other by constants. I agree with Bloch that the derivative function, group velocity, is the more sensitive function and should produce more resolution in the inversion process. The experimental phase velocities were determined with assumptions of a constant initial phase with frequency and of a specific number of radian circles that pertain to the source-station pair. A similar assumption is not required in the group velocity determination. Since ample group-velocity dispersion curves were available and provide more resolution than phase-velocity dispersion curves, this study was confined to inversion of the group-velocity dispersion curves.

Brune & Dorman (1963), McEvilly (1964) and Der & Landisman (1972) illustrate partial derivatives of Rayleigh-wave phase velocity with respect to layer shear-wave velocity, layer compressional-wave velocity, and layer density and of Love-wave phase velocity with respect to layer shear-wave velocity and layer density. The partial derivatives with respect to shear-wave velocities, are larger than the partial derivatives with respect to the other two parameters. Thus, the inversion process has considerably more resolution with shear-wave velocities than with compressional-wave velocities or densities. Both Brune & Dorman (1963) and McEvilly (1964) experienced instability when both shear-wave velocity and density were allowed to vary in a solution and both only reported on shear-wave solutions. Bloch (1969; Bloch *et al.* 1969) and James (1971b) only used shear-wave partial derivatives in their inversions. Der, Massé & Landisman (1970) found that the resolution of phase velocities was inferior to the resolution with group velocities having the same magnitude of errors.

In recent years several authors have presented theoretical discussions concerning the non-uniqueness of inversion of seismic data and concerning the resolving power of various data sets. Backus & Gilbert (1967, 1968, 1970), Backus (1970a, b, c), Jackson (1972) and Parker (1972) have treated the general problem of determining the average properties of the Earth from sets of gross earth data selected from appropriate earth functionals. Der *et al.* (1970) and Der & Landisman (1972) independently developed similar concepts, primarily for the application of inversion of surface-wave dispersion data to determine the properties of the crust and upper mantle. All of these papers develop various methods for evaluating the trade-off between resolution, stability, and errors in the data. The methods considered by these authors involve the simultaneous inversion of all parameters in the solution at one time. The method used by Bloch (1969; Bloch *et al.* 1969), James (1971b), and in this study has not been specifically treated theoretically, but the inversion for each layer is a simplified case of the larger inversion problem. The trade-offs in this study between resolution, stability, and variation of the results were made empirically based on the concepts in these papers. Resolution was achieved with many thin layers in the model FBR3 (layers are generally 4 km thick in the crust, 10 km thick in the upper mantle, and 20 km thick in the lower mantle). This high resolution sacrificed stability in that only the fundamental mode Rayleigh-wave and Love-wave dispersion curves could be used in the solution. The solutions with the higher modes had the same characteristics of high velocities or low velocities in the same layers as the fundamental mode solutions, but the layer shear-velocity values were exaggerated, i.e. unreasonably too high or too low. Also, as will be seen later, the solution starting with the top layer and proceeding down, varied in the low-velocity regions from the solution starting with the bottom layer and proceeding up. Very satisfactory stability was achieved by thickening the layers in the starting model FBR3A while maintaining the same structure. The thicker layers produced the same solution from the top as from the bottom with six modes (LR_0, LR_1, LR_2, LQ_0, LQ_1 and LQ_2) in the solution. Stability

also was achieved in the inversion process by dropping out layers for certain modes when the sum of the partial derivatives squared was smaller than an empirically selected number. In the solution of equation (8), the product $\mathbf{P}^T\mathbf{P}$ is in the denominator. This product is the sum of the partial derivatives squared for layer k. If this product is small, the solution can become too large. Originally solutions were made with no restraints, values of the sum of the partial derivatives squared were determined for layers that had unreasonable solutions, a minimum value for $\mathbf{P}^T\mathbf{P}$ was established, and new solutions were made with the program omitting layers in which $\mathbf{P}^T\mathbf{P}$ was less than the minimum value.

Each residual $\mathbf{R}_{mi}$ (equation (4)) contains some information that is allocated to the solution of $\mathbf{D}$ in equation (8). Since layers are treated individually in the method used in this study, there is a possibility of distributing a disproportionate share of this information to the layers treated in the beginning of the solution. This fact became evident when an attempt was made to establish the crust shear velocities with fundamental Rayleigh-wave and Love-wave data; and then restraining the crust to these values, to use only the same Rayleigh-wave data to establish the upper mantle shear velocities. All the information was applied in the solution for the crust and the following solution for the mantle produced meaningless results. As a consequence of this experiment, the inversion computer program was modified to allow omission of specified layers for any mode and/or to restrain any selected layer at an arbitrary value of shear-wave velocity. In general, proper use of the deletion of layers for some modes improved the solutions and conversely, almost any restraint, including the top layer, degraded the solution. Here ' improved ' and ' degraded ' are interpreted in terms of reasonableness of relative velocities in the various layers and in terms of the root-mean-square (rms) values of final residuals (equation (10)) for each mode individually and all modes collectively. To accommodate a reasonable allocation of the information in the residuals $\mathbf{R}_{mi}$ to the layers treated early in the solution, it was found necessary to weight the solution of these layers. A weighting factor of less than 1·0 calculated by the index of the layer encountered in the solution times the iteration number divided by 10 was applied for the first seven iterations. Thus, the first layer used in the solution was weighted from 0·1 to 0·7 for seven iterations, respectively, the second layer was weighted for four iterations, the third layer for three, the fourth layer for two, and the fifth through the ninth layers were weighted only for the first iteration. This weighting produced stability in the first three layers encountered in the solution that was not possible without the weighting.

Results

The results of this study are (1) a set of observed group-velocity dispersion curves for six surface-wave modes for a path across Central Mexico determined from a seismograph station with ultra-high sensitivity three-component inertial seismographs and strain seismographs, (2) statistical properties on the measurement variations from 108 earthquake-instrument pairs for the fundamental mode Rayleigh-wave and Love-wave group velocity dispersion curves; and (3) four similar models of the shear-wave velocities in the crust and upper mantle of Central Mexico.

The group-velocity dispersion curve for the fundamental mode Rayleigh-wave is plotted in Fig. 11; and the group-velocity dispersion curve for the fundamental Love-wave is plotted in Fig. 12. The central curves are the mean of the group velocities obtained from the multiple filter analysis. The other two curves in each figure are the mean plus and minus the average deviation from the mean (first moment). Statistical properties of the observations of group velocities are given in Table 4 for the fundamental Rayleigh-wave and in Table 5 for the fundamental Love-wave. The values of the sample mean in the fourth columns were smoothed with a seven point least squares

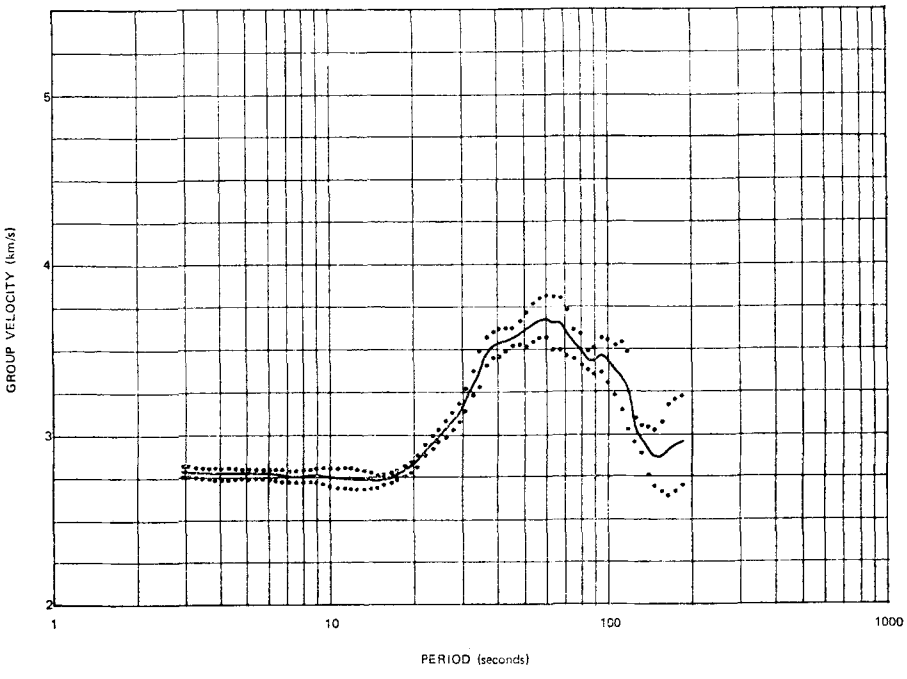

FIG. 11. Observed group-velocity dispersion curve with average deviation from the mean for fundamental mode Rayleigh wave.

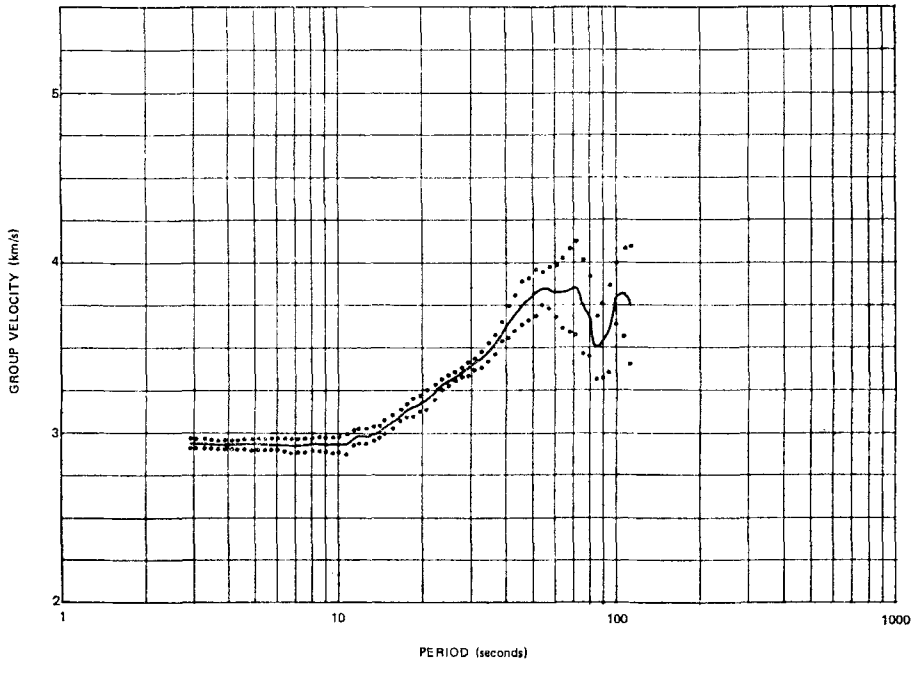

FIG. 12. Observed group-velocity dispersion curve with average deviation from the mean for fundamental mode Love wave.

Table 4

Statistics on observed group velocities Rayleigh-wave mode LR_0

Index	Period	Smooth mean	Mean	Std dev.	Median	Ave 1st moment	No. samples	Range Max	Range Min	Index
1	2·90680	2·7729	2·7721	0·0391	2·7800	0·0328	47	2·8400	2·7000	1
2	3·07472	2·7725	2·7743	0·0406	2·7800	0·0345	47	2·8600	2·7000	2
3	3·25233	2·7713	2·7706	0·0399	2·7700	0·0327	48	2·8600	2·7000	3
4	3·44021	2·7692	2·7683	0·0375	2·7650	0·0304	48	2·8500	2·7000	4
5	3·63895	2·7667	2·7671	0·0388	2·7600	0·0325	48	2·8400	2·7000	5
6	3·84916	2·7652	2·7656	0·0394	2·7600	0·0328	50	2·8400	2·6800	6
7	4·07152	2·7635	2·7630	0·0409	2·7600	0·0334	50	2·8400	2·6800	7
8	4·30672	2·7619	2·7624	0·0424	2·7600	0·0348	50	2·8500	2·6800	8
9	4·55551	2·7611	2·7606	0·0403	2·7600	0·0320	51	2·8400	2·7000	9
10	4·81867	2·7618	2·7612	0·0387	2·7600	0·0314	51	2·8600	2·7000	10
11	5·09703	2·7622	2·7625	0·0384	2·7600	0·0313	52	2·8600	2·7000	11
12	5·39147	2·7622	2·7636	0·0370	2·7600	0·0281	53	2·8500	2·7000	12
13	5·70292	2·7614	2·7602	0·0368	2·7600	0·0286	57	2·8500	2·7000	13
14	6·03237	2·7591	2·7591	0·0376	2·7600	0·0296	57	2·8600	2·7000	14
15	6·38084	2·7561	2·7571	0·0432	2·7600	0·0337	59	2·8700	2·6600	15
16	6·74945	2·7531	2·7528	0·0473	2·7600	0·0390	58	2·8700	2·6600	16
17	7·13935	2·7501	2·7500	0·0482	2·7600	0·0400	59	2·8600	2·6500	17
18	7·55177	2·7485	2·7482	0·0481	2·7500	0·0389	61	2·8600	2·6300	18
19	7·98802	2·7498	2·7488	0·0471	2·7500	0·0385	60	2·8500	2·6400	19
20	8·44947	2·7524	2·7513	0·0458	2·7600	0·0367	60	2·8600	2·6500	20
21	8·93757	2·7526	2·7551	0·0528	2·7600	0·0415	59	2·8600	2·6400	21
22	9·45387	2·7495	2·7519	0·0529	2·7600	0·0433	57	2·8600	2·6400	22
23	10·00000	2·7446	2·7419	0·0691	2·7300	0·0560	57	2·8700	2·5700	23
24	10·57768	2·7404	2·7383	0·0717	2·7200	0·0569	58	2·9000	2·5600	24
25	11·18872	2·7379	2·7386	0·0767	2·7250	0·0602	66	2·9200	2·5600	25
26	11·83507	2·7364	2·7386	0·0747	2·7400	0·0586	66	2·9100	2·5600	26
27	12·51875	2·7324	2·7321	0·0745	2·7450	0·0606	66	2·8500	2·5600	27
28	13·24193	2·7264	2·7272	0·0705	2·7400	0·0556	64	2·8600	2·5100	28
29	14·00688	2·7216	2·7211	0·0628	2·7300	0·0506	65	2·8600	2·5200	29
30	14·81603	2·7228	2·7209	0·0471	2·7100	0·0375	64	2·8500	2·6100	30
31	15·67191	2·7286	2·7284	0·0407	2·7300	0·0298	63	2·8400	2·5800	31
32	16·57724	2·7412	2·7431	0·0379	2·7400	0·0271	65	2·8200	2·5700	32
33	17·53487	2·7569	2·7558	0·0404	2·7500	0·0274	62	2·8200	2·5400	33

Table 4 (*continued*)

34	18·54781	2·7741	2·7789	0·0478	2·7700	0·0331	62	2·8700	2·5400	34
35	19·61927	2·8031	2·7993	0·0514	2·800	0·0350	60	2·8900	2·5500	35
36	20·75263	2·8455	2·8349	0·0566	2·8400	0·0389	57	2·9300	2·5700	36
37	21·95146	2·8945	2·9024	0·0501	2·9000	0·0373	51	3·0100	2·7400	37
38	23·21954	2·9441	2·9510	0·0592	2·9500	0·0422	51	3·1200	2·7500	38
39	24·56088	2·9919	2·9889	0·0558	2·9900	0·0380	45	3·2000	2·9000	39
40	25·97970	3·0302	3·0273	0·0711	3·0200	0·0480	35	3·2900	2·9100	40
41	27·48048	3·0748	3·0832	0·0756	3·0750	0·0518	28	3·3500	2·9600	41
42	29·06796	3·1350	3·1241	0·0795	3·1100	0·0574	27	3·4000	3·0300	42
43	30·74715	3·2079	3·2054	0·0839	3·2000	0·0669	26	3·4100	3·0700	43
44	32·52334	3·2983	3·3005	0·0924	3·3150	0·0705	20	3·4700	3·1200	44
45	34·40213	3·3941	3·3852	0·1392	3·4100	0·1057	21	3·6800	3·1300	45
46	36·38946	3·4678	3·4850	0·1080	3·5000	0·0860	20	3·6700	3·2700	46
47	38·49159	3·5155	3·5215	0·0998	3·5450	0·0765	20	3·6800	3·2800	47
48	40·71515	3·5417	3·5333	0·1133	3·5600	0·0833	21	3·7200	3·2200	48
49	43·06717	3·5541	3·5511	0·1004	3·5500	0·0653	19	3·7000	3·2400	49
50	46·55506	3·5708	3·5716	0·0627	3·5600	0·0532	19	3·6800	3·4600	50
51	48·18666	3·5947	3·5961	0·0810	3·5600	0·0706	18	3·7400	3·4800	51
52	50·97029	3·6225	3·6165	0·1349	3·5800	0·1047	17	3·8200	3·2800	52
53	53·91471	3·6537	3·6518	0·1365	3·6000	0·1135	17	3·8900	3·3600	53
54	57·02924	3·6701	3·6769	0·1679	3·6200	0·1194	16	4·1600	3·4600	54
55	60·32368	3·6788	3·6869	0·1947	3·6550	0·1306	16	4·2400	3·3500	55
56	63·80843	3·6689	3·6500	0·2389	3·5800	0·1585	13	4·3000	3·3200	56
57	67·49448	3·6363	3·6525	0·2463	3·5950	0·1608	12	4·2800	3·3200	57
58	71·39348	3·5941	3·5977	0·2064	3·5700	0·1331	13	4·0700	3·1500	58
59	75·51770	3·5404	3·5300	0·1357	3·5250	0·0820	10	3·8400	3·3200	59
60	79·88018	3·4809	3·4944	0·1650	3·4800	0·0933	9	3·8500	3·2100	60
61	84·49466	3·4524	3·4314	0·0776	3·4200	0·0586	7	3·5500	3·3200	61
62	89·37571	3·4438	3·4329	0·0988	3·4300	0·0800	7	3·5600	3·3200	62
63	94·53873	3·4341	3·4583	0·1408	3·4500	0·0983	6	3·6300	3·2300	63
64	100·00000	3·4252	3·4260	0·1760	3·4200	0·1280	5	3·6000	3·1600	64
65	105·77675	3·4012	3·3750	0·2009	3·3600	0·1450	4	3·6300	3·1500	65
66	111·88722	3·3149	3·3375	0·2510	3·2900	0·1975	4	3·6600	3·1100	66
67	118·35067	3·2028	3·2500	0·3051	3·1100	0·2333	3	3·6000	3·0400	67
68	125·18750	3·0780	3·0200	0·0990	3·0200	0·0700	2	3·0900	2·9500	68
69	132·41928	2·9586	2·9600	0·1273	2·9600	0·0900	2	3·0500	2·8700	69
70	140·06882	2·8812	2·8950	0·2051	2·8950	0·1450	2	3·0400	2·7500	70
71	148·16025	2·8662	2·8550	0·2333	2·8550	0·1650	2	3·0200	2·6900	71

Table 5

Statistics on observed group velocities Love-wave mode LQ_0

Index	Period	Smooth mean	Mean	Std dev.	Median	Ave 1st moment	No. samples	Range Max	Range Min	Index
1	2·90680	2·9351	2·9350	0·0350	2·9400	0·0267	24	3·0000	2·8600	1
2	3·07472	2·9347	2·9346	0·0322	2·9400	0·0271	24	2·9800	2·8600	2
3	3·25233	2·9337	2·9348	0·0343	2·9400	0·0288	25	2·9800	2·8600	3
4	3·44021	2·9323	2·9308	0·0336	2·9400	0·0285	26	2·9600	2·8600	4
5	3·63895	2·9308	2·9304	0·0330	2·9400	0·0263	27	2·9600	2·8400	5
6	3·84916	2·9285	2·9307	0·0332	2·9400	0·0259	27	2·9800	2·8400	6
7	4·07152	2·9287	2·9274	0·0365	2·9400	0·0270	27	2·9800	2·8200	7
8	4·30672	2·9283	2·9259	0·0383	2·9400	0·0300	27	2·9800	2·8200	8
9	4·55551	2·9281	2·9317	0·0395	2·9400	0·0314	29	2·9800	2·8200	9
10	4·81867	2·9286	2·9272	0·0406	2·9400	0·0338	29	2·9800	2·8300	10
11	5·09703	2·9279	2·9276	0·0367	2·9400	0·0286	29	2·9600	2·8300	11
12	5·39147	2·9274	2·9276	0·0388	2·9400	0·0286	29	2·9600	2·8200	12
13	5·70292	2·9275	2·9261	0·0399	2·9400	0·0297	31	2·9700	2·8200	13
14	6·03237	2·9253	2·9287	0·0406	2·9400	0·0300	32	2·9800	2·8200	14
15	6·38084	2·9230	2·9219	0·0460	2·9400	0·0355	31	2·9800	2·8100	15
16	6·74945	2·9203	2·9190	0·0496	2·9400	0·0410	30	2·9800	2·8000	16
17	7·13935	2·9206	2·9210	0·0516	2·9400	0·0416	31	3·0200	2·8000	17
18	7·55177	2·9242	2·9213	0·0485	2·9300	0·0387	31	3·0200	2·7900	18
19	7·98802	2·9280	2·9314	0·0553	2·9400	0·0386	29	3·0700	2·7800	19
20	8·44947	2·9285	2·9297	0·0500	2·9200	0·0383	29	3·0300	2·7900	20
21	8·93757	2·9289	2·9286	0·0499	2·9200	0·0407	28	3·0200	2·8100	21
22	9·45387	2·9238	2·9236	0·0552	2·9200	0·0464	28	3·0200	2·8000	22
23	10·00000	2·9287	2·9311	0·0517	2·9200	0·0456	27	3·0300	2·8600	23
24	10·57768	2·9420	2·9285	0·0680	2·9500	0·0578	27	3·0300	2·7600	24
25	11·18872	2·9577	2·9676	0·0540	2·9800	0·0432	25	3·0600	2·8600	25
26	11·83507	2·9714	2·9779	0·0534	2·9900	0·0413	24	3·0600	2·8700	26
27	12·51875	2·9843	2·9784	0·0500	2·9900	0·0392	25	3·0500	2·8700	27
28	13·24193	2·9918	2·9909	0·0597	3·0100	0·0443	23	3·0500	2·8100	28
29	14·00688	3·0088	3·0092	0·0575	3·0250	0·0377	26	3·0700	2·7900	29
30	14·81603	3·0347	3·0329	0·0726	3·0350	0·0429	28	3·2500	2·7800	30
31	15·67191	3·0659	3·0652	0·0630	3·0600	0·0393	29	3·3200	2·9400	31
32	16·57724	3·0973	3·0987	0·0620	3·0950	0·0353	30	3·3500	2·9500	32

Table 5 (*continued*)

33	17·53487	3·1256	3·1294	0·0599	3·1200	0·0381	31	3·3500	2·9800	33
34	18·54781	3·1469	3·1474	0·0712	3·1400	0·0529	31	3·3500	2·9900	34
35	19·61927	3·1684	3·1687	0·0662	3·1650	0·0513	30	3·3400	3·0300	35
36	20·75263	3·1987	3·1900	0·0726	3·2000	0·0568	31	3·3300	3·0300	36
37	21·95146	3·2350	3·2351	0·0693	3·2400	0·0449	35	3·3300	2·9400	37
38	23·21954	3·2740	3·2822	0·0384	3·2800	0·0289	36	3·3600	3·1900	38
39	24·56088	3·3082	3·3051	0·0394	3·3100	0·0292	37	3·3900	3·2000	39
40	25·97970	3·3327	3·3356	0·0319	3·3400	0·0239	36	3·4300	3·2800	40
41	27·48048	3·3530	3·3514	0·0361	3·3450	0·0292	36	3·4500	3·2700	41
42	29·06796	3·3751	3·3750	0·0640	3·3700	0·0365	40	3·7000	3·2700	42
43	30·74715	3·4010	3·4011	0·0733	3·3950	0·0433	36	3·7400	3·2700	43
44	32·52334	3·4344	3·4317	0·0789	3·4300	0·0478	36	3·7700	3·2600	44
45	34·40213	3·4733	3·4774	0·0859	3·4600	0·0580	35	3·7800	3·3000	45
46	36·38946	3·5240	3·5207	0·0853	3·5050	0·0593	30	3·7600	3·4000	46
47	38·49159	3·5830	3·5771	0·0984	3·5500	0·0790	31	3·7900	3·4300	47
48	40·71515	3·6455	3·6510	0·1282	3·6200	0·0983	29	3·9800	3·4000	48
49	43·06717	3·7054	3·7064	0·1535	3·6750	0·1064	28	4·1300	3·3400	49
50	45·55506	3·7549	3·7573	0·1954	3·7200	0·1258	26	4·4000	3·2700	50
51	48·18666	3·7936	3·7908	0·2147	3·7600	0·1288	25	4·5300	3·2100	51
52	50·97029	3·8265	3·8222	0·2469	3·8200	0·1387	23	4·6400	3·1600	52
53	53·91471	3·8427	3·8485	0·1273	3·8100	0·0970	20	4·1400	3·6800	53
54	57·02924	3·8446	3·8548	0·1528	3·8300	0·1229	21	4·1900	3·6100	54
55	60·32368	3·8371	3·8289	0·1937	3·8400	0·1505	19	4·1500	3·4200	55
56	63·80843	3·8434	3·8250	0·2666	3·8750	0·2081	16	4·2100	3·3200	56
57	67·49448	3·8374	3·8359	0·3075	3·8600	0·2453	17	4·3400	3·2500	57
58	71·39348	3·8248	3·8556	0·3342	3·8250	0·2806	16	4·4300	3·3400	58
59	75·51770	3·7466	3·7433	0·3549	3·7100	0·2767	15	4·4800	3·2200	59
60	79·88018	3·6425	3·6785	0·3206	3·5900	0·2300	13	4·4800	3·2400	60
61	84·49466	3·5478	3·4978	0·2395	3·4300	0·1889	9	3·8200	3·0800	61
62	89·37571	3·5611	3·5400	0·2913	3·4900	0·2244	9	3·9000	2·9900	62
63	94·53873	3·6432	3·6088	0·3257	3·6350	0·2588	8	4·0100	3·0400	63
64	100·00000	3·7461	3·8183	0·2452	3·8400	0·1883	6	4·1500	3·5400	64
65	105·77675	3·8078	3·8200	0·3904	3·8000	0·2667	3	4·2200	3·4400	65

smoothing (Lanczos 1956) to obtain the values in the third columns. The smoothed sample mean values were used in the inversions.

The smoothed values are essentially within 0·01 km s^{-1} or less from the mean values and are considered to be the better set of experimental group velocities. The sample standard deviations are given in the fifth column. In an attempt to improve the data set by removing outliers, the data were truncated at plus and minus one standard deviation in a manner similar to that used with body-wave data (Freedman 1966, 1968; Tucker, Herrin & Freedman 1968). When the standard deviation of the whole population was estimated from the standard deviation of the truncated sample and the $p(k)$ factor for a normal distribution (Freeman 1966), larger estimates of the standard deviation were obtained than given in the table. Since 60 or more samples are available at many of the periods, the sample population should be a good representation of the whole population. Two conclusions are apparent: truncation of the data set is not valid and should not be used (that is, there are no samples that can be statistically deemed as outliers) and the distribution of samples is tighter than a normal distribution. The sample data set used in this study has not been truncated. The tight statistical distribution is the result of the resolution of the multiple filter analysis and of the diligence used in the data processing.

Claerbout & Muir (1973) have proposed the use of the sample median instead of the sample mean and the absolute value of the sample variation from the median instead of the square of the difference between a sample and the arithmetic mean. The sample median and the average sample variation from the mean are given in Tables 4 and 5. For these data, the medians are almost identical to the means. This identity is the result of a symmetrical two-sided distribution with no skewness to either early or late times. The errors in the observed group velocities quantized by the sample standard deviation and the average deviation from the mean include errors from (1) origin time, (2) hypocentre location, (3) initial phase of the source, (4) station timing errors, (5) non-great circle propagation paths, (6) interference from lateral refractions, (7) incomplete separation of modes, (8) incorrect digitizing start times and/or sampling rates, (9) mistakes in entering parameters into computer programs, (10) unknown bugs in computer programs, (11) incorrect picks of maxima on the multiple filter analysis output, (12) bias in the interpretation of the dispersion curve. Despite these sources of errors, the average deviation from the mean was between about 0·025 and 0·060 km s^{-1} for both Rayleigh waves and Love waves for periods up to 35 s. At longer periods, the average deviation was about 0·060 to 0·160 km s^{-1} for Rayleigh waves and between about 0·060 and 0·281 km s^{-1} for Love waves. At the shorter periods, the Love-wave deviations are smaller than the Rayleigh-wave deviations, but at the longer periods, the situation is reversed. By inspection of the seismogram in Fig. 2, it can be seen that, at this epicentral distance, the fundamental Love wave begins about 40 s after the *S*-wave arrival and among the higher mode Love-wave arrivals. Apparently, this mixture of modes has confused the analysis with the resulting large deviations from the mean among the 15–20 samples at each period from 45 to 75 s. Similar but more serious mixture of Love modes was observed by James (1971a) in South America and by Thatcher & Brune (1973) in Baja California.

Only limited data on surface-wave dispersion in Mexico are available in the literature. These data, all for fundamental Rayleigh waves, from Papazachos (1964), Santo (1965), Tarr (1969) and Thatcher & Brune (1973), are plotted as data points in Fig. 13 along with the LR_0 curve from this study. Agreement among the data points is exceptional for all paths except the Gulf of California–TUC and Baja California paths of Thatcher & Brune (1973).

Several group-velocity dispersion curves for the first higher mode Rayleigh wave LR_1 and the second higher mode Rayleigh wave LR_2 are plotted in Fig. 14. Several group-velocity dispersion curves for the first higher mode Love wave LQ_1 and the

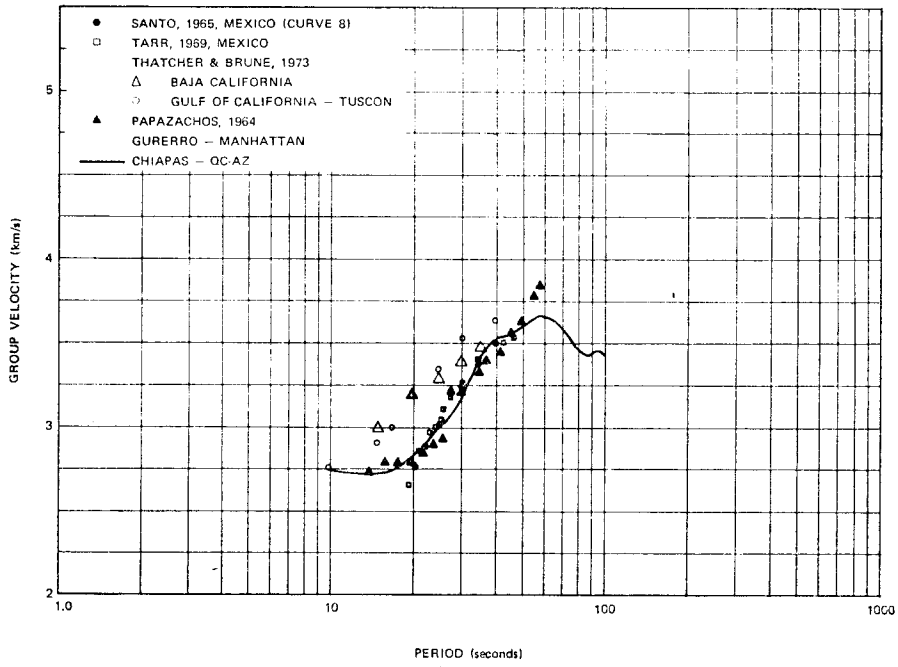

FIG. 13. Observed group-velocity dispersion curve for fundamental mode Rayleigh wave from the literature.

second higher mode Love wave LQ_2 are plotted in Fig. 15. The scatter in group-velocity of the higher modes is greater than for the fundamental modes. In the steep portions of the curves, it is better to consider the variation as taking place in period rather than in group velocity. Some energy from the higher modes can be seen, but is not contoured, in the multiple filter analyses illustrated in Figs 3, 4 and 5 which are plotted in terms of normalized linear amplitudes. The curves in Figs 14 and 15 were derived from the plots of normalized decibel amplitudes that show more detail for the smaller amplitudes. Because of the bias that the large slopes might introduce into numerical averages and because of lack of success with erroneously determined higher mode dispersion curves, I decided to use a set of typical dispersion curves for the higher modes that were actual observations from the real world and not average numbers that could have been masticated by numerical manipulation. The selected curves are shown with bolder lines in Figs 14 and 15. They were chosen as medians by visual inspection. The curves in Figs 14 and 15 were determined from the data by picking amplitude maxima in the multiple filter analysis in the general shape of theoretical dispersion curves calculated from preliminary solutions using the fundamental modes of Rayleigh wave and Love wave. Information on additional higher modes is contained in the data, but no satisfactory method was discovered of establishing the correct mode for the several prominent energy packets. This statement is especially applicable in the vicinity of the group velocity of 4·50 km s^{-1}. As can be seen in Fig. 2, this is the arrival time of the *S* wave. Tolstoy & Usdin (1953) and Satô, Usami & Landisman (1968) provide an understanding of the method by which normal modes can be summed to generate body waves. Theoretical group-velocity dispersion curves for the first five higher modes calculated for model FBR3 had a well-defined flat region between group velocities of 4·00 and 4·20 km s^{-1} and another less well-defined flat region between group velocities of 3·25 and 3·50 km s^{-1}. Using

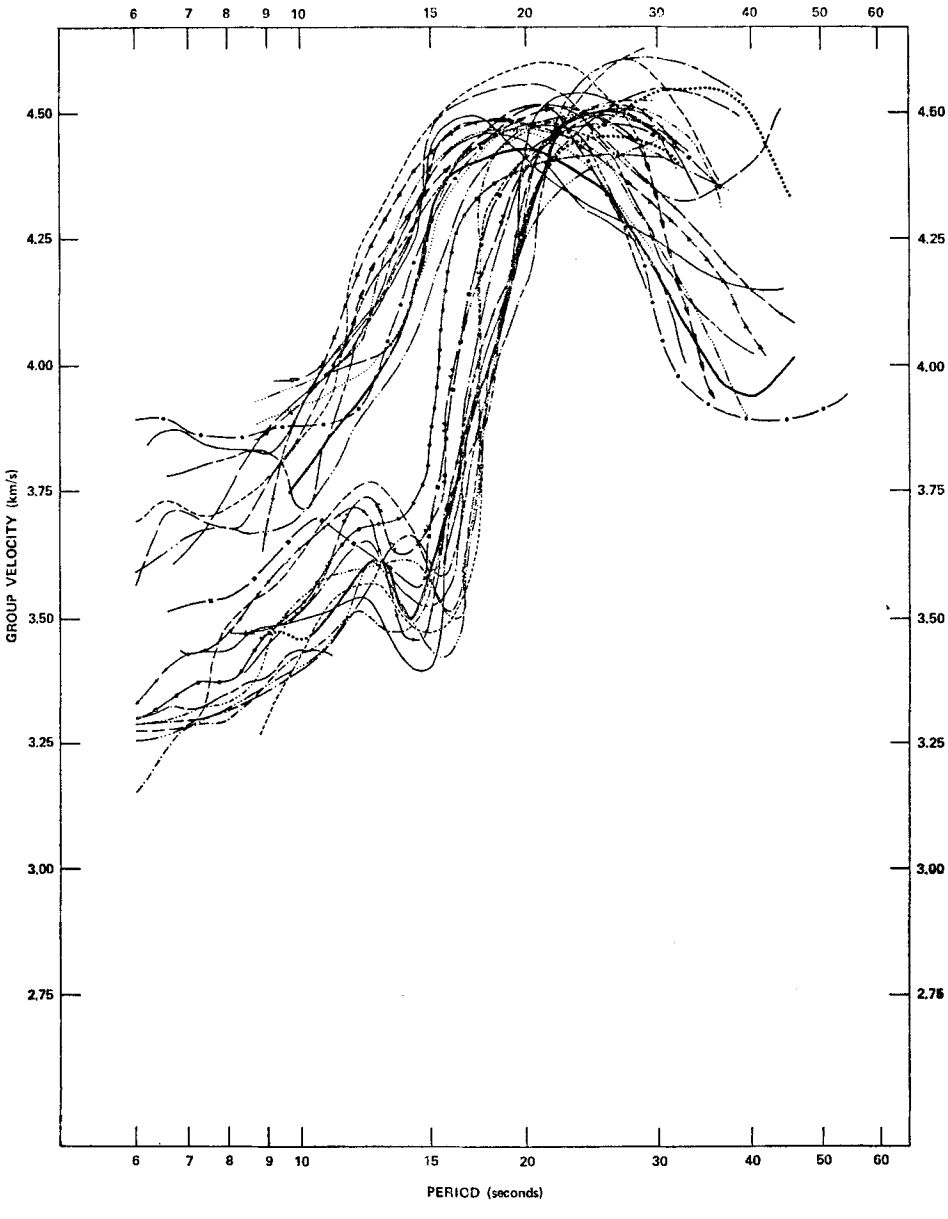

FIG. 14. Observed group-velocity dispersion curves for first higher and for second higher Rayleigh wave.

ray theory, the first flat region corresponds to the *S*-wave arrival. Similarly in the multiple filter analyses of this study, energy is detected over a large period range in the vicinity of $4{\cdot}5\,\mathrm{km\,s^{-1}}$. The velocity of the faster flat region in the theoretical curves is controlled by the $4{\cdot}50\,\mathrm{km\,s^{-1}}$ shear-wave velocity in the lid of the mantle. The second flat in the theoretical curves corresponds to the Lg and Rg arrivals and is controlled by the $3{\cdot}80\,\mathrm{km\,s^{-1}}$ shear-wave velocity in the bottom layer of the crust. Based on a qualitative comparison with Figs 14 and 15, the lid of the mantle should

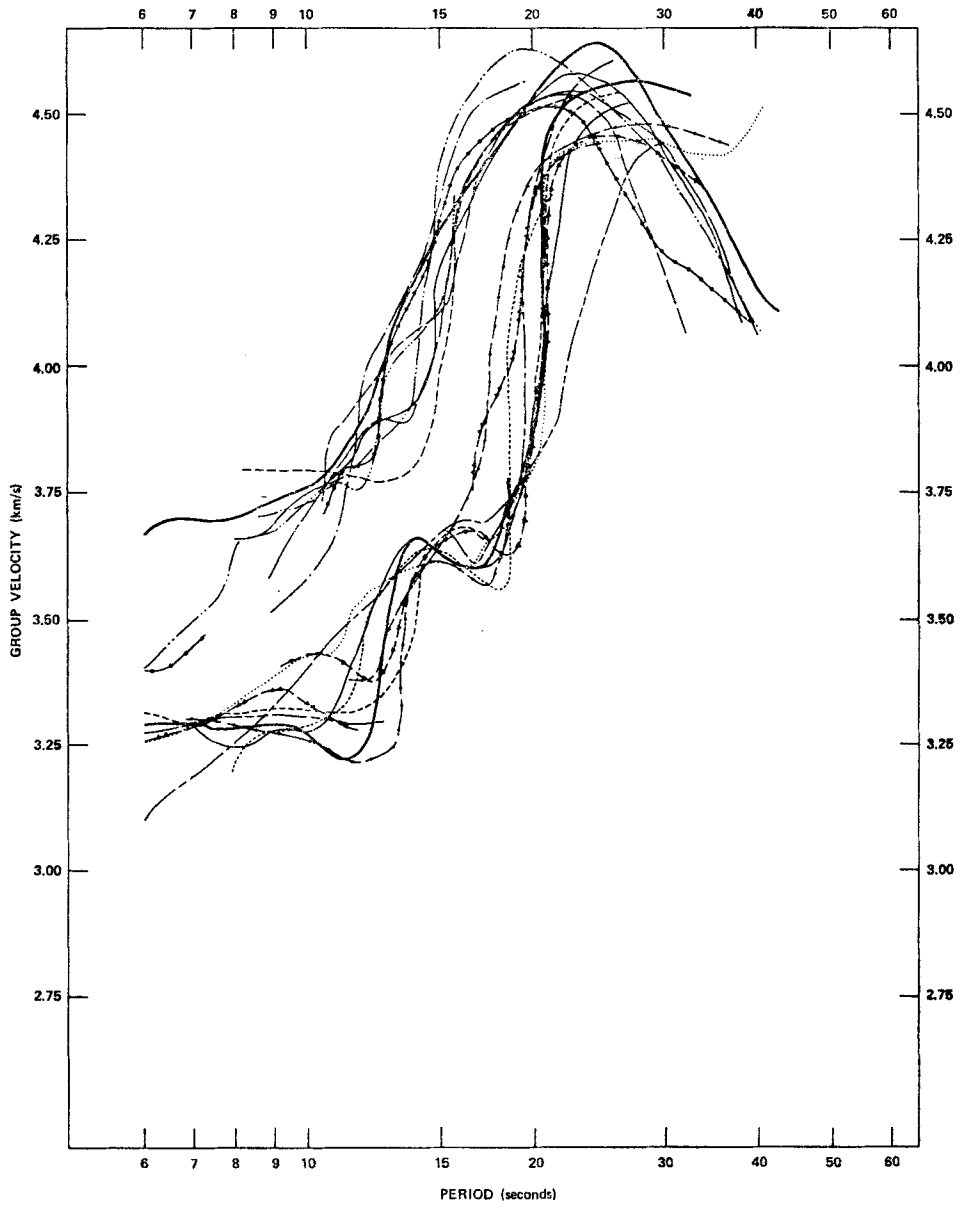

FIG. 15. Observed group-velocity dispersion curves for first higher and for second higher Love wave.

have a shear-wave velocity greater than 4·5 km s^{-1} and the bottom layer in the crust should have a shear-wave velocity greater than 3·6 km s^{-1}.

A considerable number of inversions were made with various combinations of modes and with various combinations of data sets. The majority of the models from the solutions had the same general shape with low velocity zones in the same layers and with fast velocities in the same layers. Four preferred models are presented below. Two models (numbers 1 and 2) were generated from solutions with the high resolution

Table 6

Modes, period ranges and number of layers used in the inversion for models 1, 2, *A*1 *and A*2

Model 1 and 2			Model A1 and A2		
Mode	Period range	No. of layers	Mode	Period range	No. of layers
LR_0	10·0–71·4	28	LR_0	10·0–71·4	14
LQ_0	10·0–71·4	28	LR_1	15·7–30·7	14
			LR_2	9·45–40·7	14
			LQ_0	10·0–71·4	14
			LQ_1	14·8–34·4	14
			LQ_2	8·4–40·7	14

starting model FBR3 and the other two models (numbers A1 and A2) were generated from solutions with the starting model FBR3A that produced more stable results. Solutions for models 1 and A1 begin the inversion with the top layer; solutions for models 2 and A2 begin the inversion with the bottom layer. The modes, period ranges, and the number of layers used in these inversions are given in Table 6. The shear-wave velocities for models 1 and 2 along with those for model FBR3 are given in Table 7 for the upper 100 km of crust and upper mantle. These velocities are plotted in Fig. 16. The partial derivatives are small for layers 20–28 for the fundamental modes (see Figs 7 and 8) and the model 1 and 2 velocities are unrealistic for depths greater than 100 km and have not been presented. The shear-wave velocities for models A1 and A2 and model FBR3A are given in Table 8. The upper 100 km of crust and upper mantle are plotted in Fig. 17. The entire models are plotted in Fig. 18.

The Rayleigh-wave group velocity dispersion curves calculated from the four models are plotted in Fig. 19 with the observed smoothed mean plus and minus the average deviation from the mean for the fundamental mode and with the observed first and second higher mode 'median' dispersion curves. Similar curves are plotted in Fig. 20 for the Love-wave modes. The group velocities from the high resolution models 1 and 2 and for the fundamental Love wave for models A1 and A2 all lie well within the variation band of the observed fundamental modes. A comparison of Figs 19 and 20 with Figs 14 and 15 provides similar data for the higher modes. The second higher modes were fitted very well by the inversions and generally lie within the band of observations. The first higher modes were not fitted as well. Some of the variations from the high modes propagated into the residuals for the fundamental modes, especially the Rayleigh. The use of all six modes has provided a sharpening of the resolution kernel (Der *et al.* 1970; Jackson 1972), but the inclusion of the higher mode data with a larger variance has increased the residuals (Jackson 1972).

Discussion of results

The shear-wave velocity structures of the four inversion models in Figs 16–18 represent the lowest shear-wave velocities of any area of the world studied to date. These velocities are probably representative of other similar regions with high heat flow and high uplifted plateaus. In the following paragraphs, the physical properties of the velocities will be presented and then will be interpreted in terms of the generalized petrology, a representative geotherm, partial melting, and phase changes within the materials. Differences between *S*-wave travel times through the models are compared with *S*-wave station residuals.

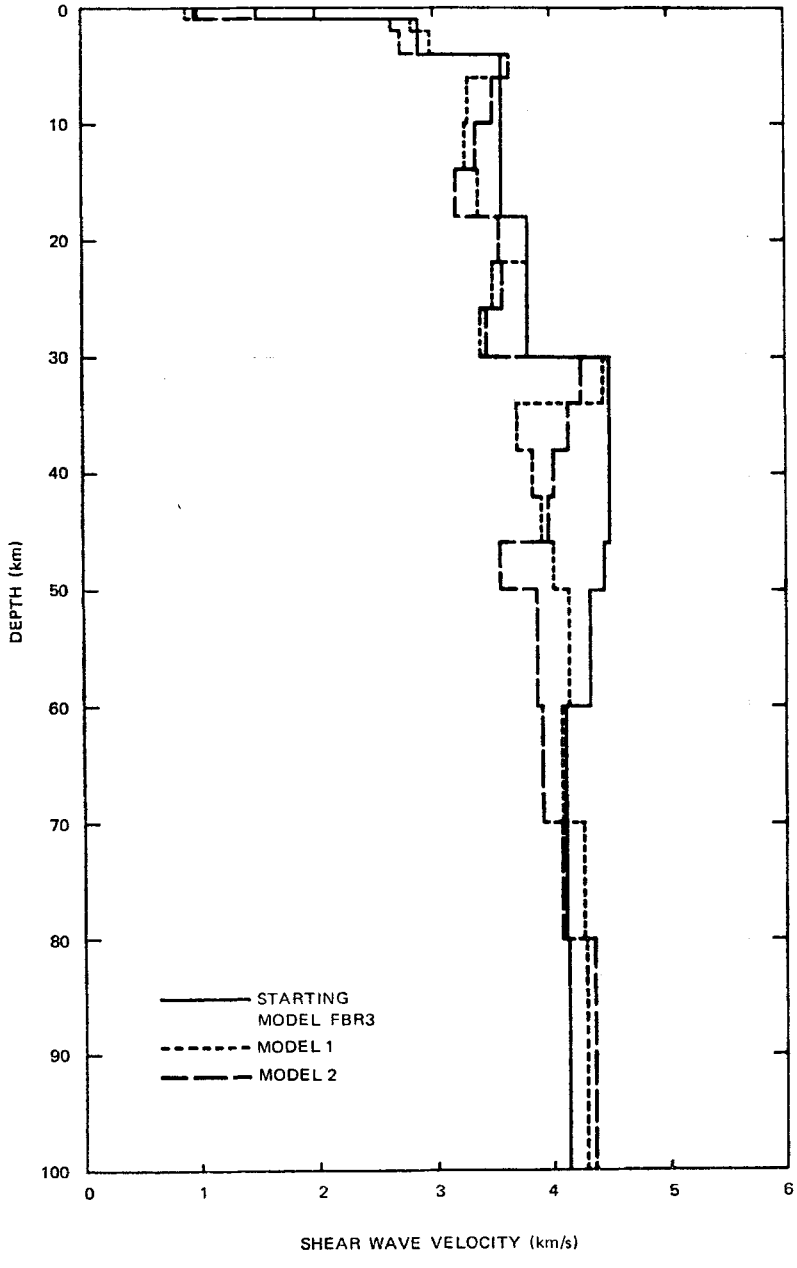

FIG. 16. Upper 100 km shear-wave structure from inversion of fundamental mode Rayleigh-wave and Love-wave group velocities with starting model FBR3.

The inversion models 1 and 2 (Table 7, Fig. 16) have a four-layer 30 km thick crust with velocities corresponding to: a low-velocity sedimentary layer, a sedimentary rock layer, a granitic layer with a low velocity zone, and a basaltic layer with a low velocity zone. The mantle has a thin 4 km lid with a normal shear-wave velocity. Immediately below the lid partial melting occurs. (Partial melting percentages given in this part of the paper for the mantle are based on the shear velocities calculated by Birch (1969) based on spherical nodules of basalt melting along the solidus in a host

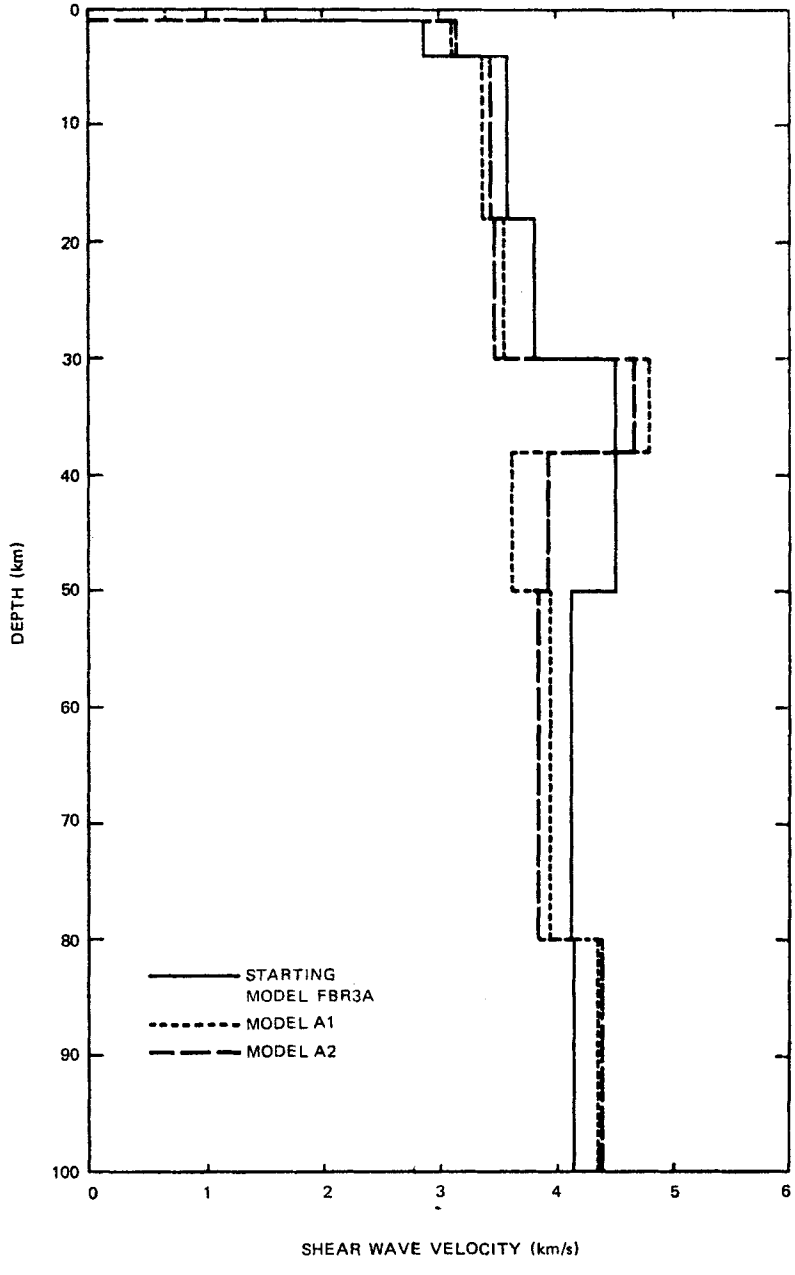

FIG. 17. Upper 100 km shear-wave velocity structure from inversion of fundamental mode, first higher mode, and second higher mode Rayleigh-wave and Love-wave group velocities with starting model FBR3A.

of olivine. Actual partial melting probably occurs in a planar structure along grain boundaries and the actual percentage of melt for the same shear-wave velocity may be significantly less than with the Birch spherical melt model.) Model 1 drops to a very low shear-wave velocity at a depth of 34 km implying an 18 per cent partial melting that gradually decreases to 5 per cent melt at the 100 km depth. Model 2 grades into

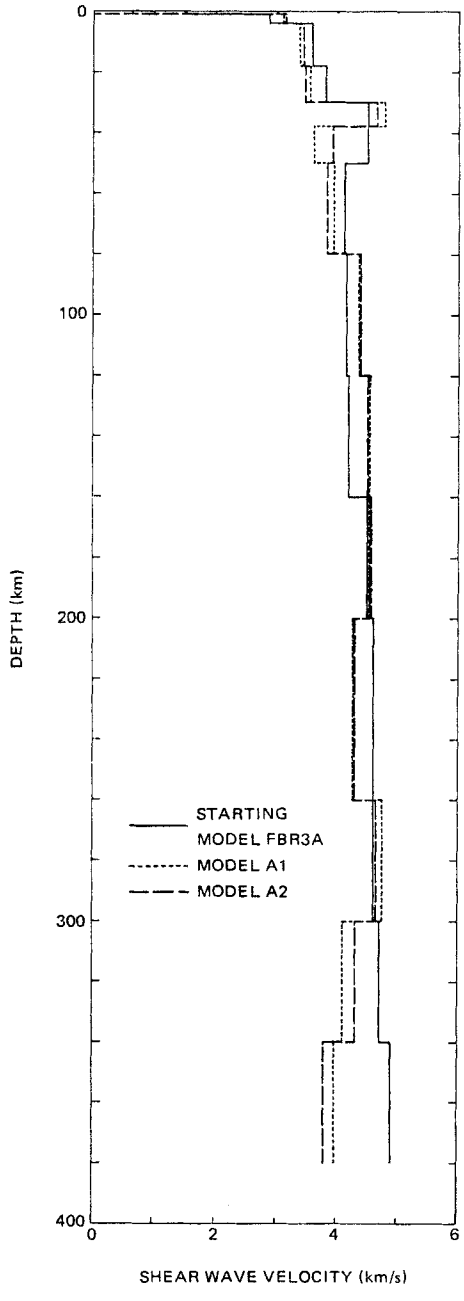

FIG. 18. Shear-wave velocity structure from inversion of fundamental mode, first higher mode, and second higher mode Rayleigh-wave and Love-wave group velocities with starting model FBR3A.

the lowest velocity that corresponds to 20 per cent partial melting at depths of 46–50 km. Model 2 decreases to about the same velocity and the same 5 per cent melt as model 1 at the 100 km depth. At depths below 100 km, models 1 and 2 have unrealistic shear-wave velocities. The partial derivatives of group velocity with respect to layer shear-wave velocity are small for the fundamental modes for the layers

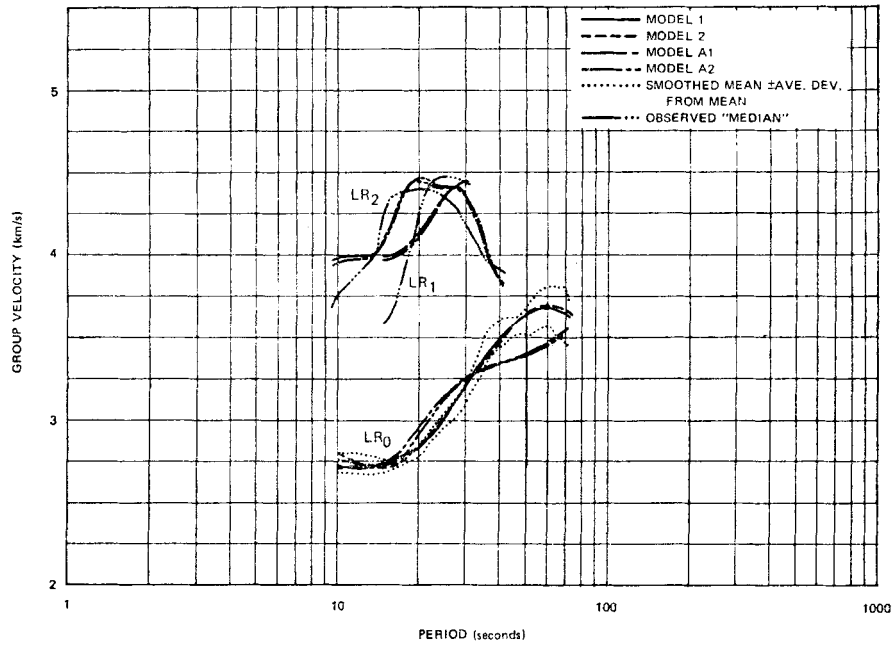

FIG. 19. Rayleigh-wave group-velocity dispersion curves: calculated from model 1, 2, A1 and A2, observed fundamental mode smoothed mean ± average deviation from the mean, and observed ' median ' higher modes.

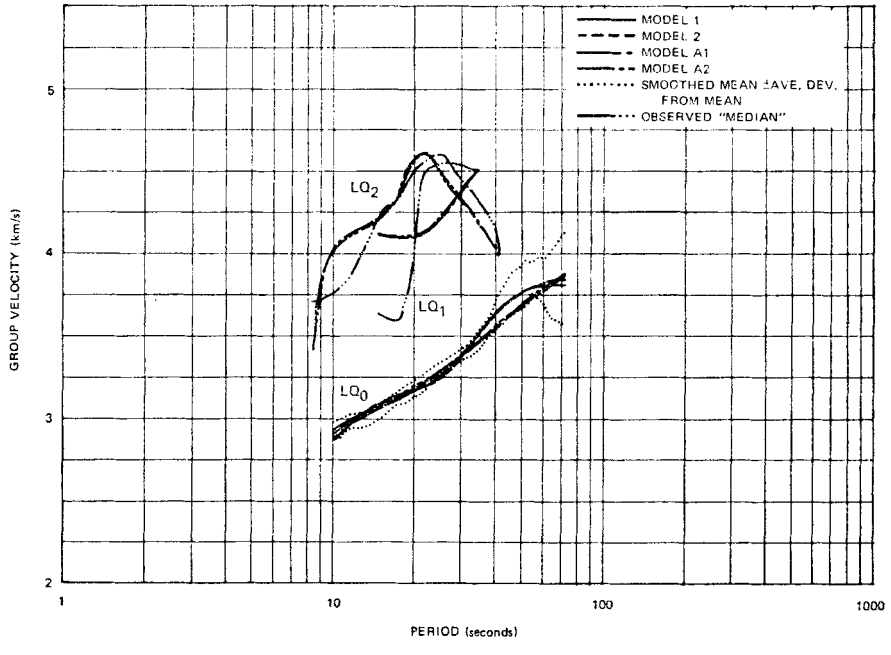

FIG. 20. Love-wave group-velocity dispersion curves: calculated from model 1, 2, A1 and A2, observed fundamental mode smoothed mean ± average deviation from the mean, and observed ' median ' higher modes.

Table 7

Shear-wave velocities for starting model FBR3 and inversion models 1 and 2

Layer No.	Depth at bottom (km)	Thickness (km)	Shear-wave velocity (km s^{-1}) Starting model FBR3	Model 1	Model 2
1	1	1	1·50	0·896	0·980
2	2	1	2·87	2·817	2·630
3	4	2	2·87	2·974	2·709
4	6	2	3·58	3·646	3·645
5	10	4	3·58	3·296	3·503
6	14	4	3·58	3·269	3·359
7	18	4	3·58	3·377	3·177
8	22	4	3·80	3·799	3·542
9	26	4	3·80	3·487	3·577
10	30	4	3·80	3·394	3·442
11	34	4	4·50	4·428	4·263
12	38	4	4·50	3·698	4·137
13	42	4	4·50	3·823	4·039
14	46	4	4·50	3·902	3·968
15	50	4	4·47	4·016	3·555
16	60	10	4·33	4·147	3·874
17	70	10	4·12	4·102	3·920
18	80	10	4·12	4·270	4·112
19	100	20	4·13	4·283	4·372

Table 8

Shear-wave velocities for starting model FBR3A and inversion models A1 and A2

Layer No.	Depth at bottom (km)	Thickness (km)	Shear-wave velocity (km s^{-1}) Starting model FBR3A	Model A1	Model A2
1	1	1	1·50	0·643	0
2	4	3	2·87	3·107	3·139
3	18	14	3·58	3·368	3·427
4	30	12	3·80	3·544	3·458
5	38	8	4·50	4·783	4·646
6	50	12	4·50	3·601	3·923
7	80	30	4·12	3·929	3·828
8	120	40	4·14	4·349	4·374
9	160	40	4·17	4·521	4·517
10	200	40	4·50	4·539	4·542
11	260	60	4·609	4·267	4·275
12	300	40	4·609	4·750	4·624
13	340	40	4·72	4·092	4·305
14	380	40	4·89	3·962	3·780

20–28 that are at depths greater than 100 km (see Figs 7 and 8). These solutions lost resolution for the thin layers of these models at depths greater than 100 km, and the results have not been presented.

Inversion models A1 and A2 (Table 8, Figs 17 and 18) have similar features to models 1 and 2. The crust has four layers, but the thicker layers eliminate the possibility of low velocity zones. However, the velocities are low for the granitic and basaltic layers, and are representative of the velocities in the middle of the LVZ's of

models 1 and 2, lending support to their existence. The mantle has as thin a lid as the model will allow—8 km. This lid in both models has the high velocities that were expected based on the 4·5 km s^{-1} flat region for the higher modes (Figs 14 and 15). Immediately below the lid the models have low velocity zones. Model A1, similar to model 1 that also started with the top layer, decreases to a velocity corresponding to 20 per cent partial melt between depths of 38 and 50 km, then grades up to a velocity indicating 5 per cent partial melt at depths of 80–120 km. Model A2, similar to model 2 that also started with the bottom layer, grades into a 16 per cent partial melt at depths between 50 and 80 km and then the velocity increases to that related to 5 per cent melt at depths of 80 to 120 km. Models A1 and A2 differ by only 0·003 to 0·025 km s^{-1} at depths between 80 and 260 km and follow each other closely to the bottom of the models at the 380 km depth. Models A1 and A2 have a low velocity zone at depths between 200 and 260 km. Also, there is no sharp velocity increase at the 160 km depth. Below the 300 km depth models A1 and A2 enter still another LVZ. The Ibrahim & Nuttli (1967, also Nuttli 1969) model has a LVZ at depths between 341 and 391 km with a minimum of 4·40 km s^{-1} at 371 km. One of the Hales & Roberts (1970) models (SLUTD1) retained the Ibrahim and Nuttli depths, but it required a minimum velocity of 4·10 km s^{-1}. The other Hales and Roberts model (SLUTD2) did not have this LVZ, but required an exceptionally sharp increase in velocity at the depth of 391 km. All the other models given in the literature and shown in Fig. 6 have large velocity gradients near the 400 km depth.

These physical velocity features of the four inversion models now will be interpreted in terms of a representative geotherm and of the melting temperatures of representative rocks combined with a solid–solid phase change below 380 km depth. Herrin (1972) was able to create models of the Canadian Shield and the Basin and Range that had consistent mineralogy between the two provinces, but that differed only in the temperatures between the surface and a depth of about 400 km. Similarly, the majority of the velocity structure of the inversion models can be explained by the geotherm. A heat flow model was established and temperatures were calculated for several depths. The heat flow along this path is high and a surface heat flow of about $2{\cdot}4 \times 10^{-6}$ cal cm^{-2} s is probably representative (D. D. Blackwell 1974, private communication). The heat flow model is based on a surface layer of constant heat generating material and a constant mantle heat flow (Birch, Roy & Decker 1968). The parameters assumed for calculation of the central Mexico geotherm are given in Table 9 and the temperatures are given in Table 10. For comparison, the Basin and Range model of Blackwell (1971) with the highest temperatures is also given in Tables 9 and 10. With the higher heat flow and similar conductivities, the central Mexico geotherm model is seen to be higher than the Basin and Range geotherm. The central Mexico geotherm is plotted in Fig. 21 on a part of the diagram of pressure and temperature fields for the petrologic model of a mantle of Pyrolite III composition taken from Green & Ringwood (1970). The oceanic and pre-Cambrian shield geotherms from Clark & Ringwood (1964) are included for comparison. The central Mexico geotherm and the Pyrolite III models substantiate: (1) the need for a thin, solid lid to the mantle, and (2) the requirement for partial melting in the uppermost portions of the mantle. The actual geotherm will follow the solidus from the beginning of melt to a depth at which the geotherm is lower than the solidus. The models of Table 9 and the temperatures given in Table 10 do not reflect melting and are not representative of the thermal regime below depths of about 35 km. To represent a central Mexico geotherm without melting, a line has been sketched in the figure using the general shape of the other two geotherms and approaching the same temperatures at about a 400 km depth. This sketched line is seen to cross the Pyrolite III solidus in the vicinity of the 180 km depth. However, both the geothermal model and the mineralogical model are subject to large unknowns at these pressures and temperatures. The depth of 260 km from models A1 and A2 has a larger velocity discontinuity

Table 9

Models for temperature-depth calculations

Model	Surface heat flow $\frac{\mu cal}{cm^2\ s}$	Mantle heat flow $\frac{\mu cal}{cm^2\ s}$	Depth of heat generating layer (km)	Heat generation $\frac{10^{-13}\ cal}{cm^3\ s}$	Depth to layer 2 (km)	Depth to mantle (km)	Thermal conductivity 10^{-3} cal $cm^{-1}\ s^{-1}\ °C^{-1}$ layer 1	layer 2	mantle
Central Mexico Basin and Range 1 (Blackwell 1971)	2·4	1·9	10	5·0	18	30	6·5	5·0	10·0
	1·90	1·37	10	5·3	10	30	6·5	5·0	—

Table 10

Temperature versus depth for models of Table 9

Depth (km)	Temperature (°C) Central Mexico	Basin and Range 1
0	0	0
5	175	136
10	331	252
15	477	389
20	641	526
25	831	663
30	1021	800
35	1116	937
40	1211	1074
45	1306	1211
50	1401	1348

that probably represents the bottom of the melt layer. Based on Fig. 21, the discontinuities at the 70 and 80 km depths in models 1 and 2 and at the 80 km depth in models A1 and A2 may represent the phase change from pyroxene pyrolite with a spinel and pyroxene mixture to garnet pyrolite with a garnet and olivine mixture. If this interpretation is correct, it suggests at least a 6 per cent alumina content in a pyrolite mantle. An alternate interpretation in terms of water content is presented in the next paragraph.

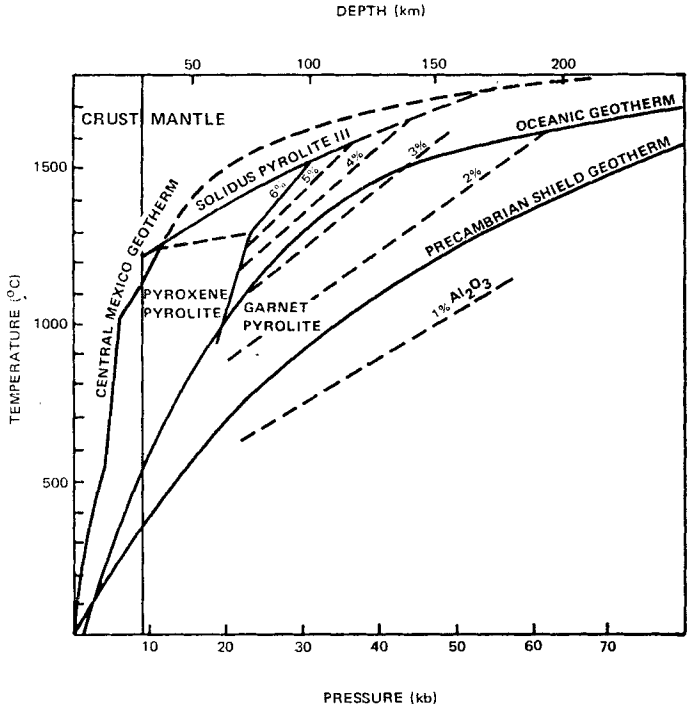

FIG. 21. Central Mexico geotherm model diagrammed with pressure, temperature, and petrologic model of mantle of Pyrolite III composition after Green & Ringwood (1970), with oceanic and Precambrian shield geotherms after Clark & Ringwood (1964).

The sharp discontinuity, the extreme low velocities, and the apparent high percentages of partial melting (based on Birch's velocities) just under the mantle lid can be explained fully in terms of the geotherm. However, fluid (water) pressure may be a significant contributor to the extent of the decrease in velocities. Anderson & Sammis (1970) have reasoned that the upper boundary of melting is also at the region of instability of the hydrous mineral phases and of the first appearance of free water with depth. A small amount of water (0·1 per cent) can lower the melting temperature by as much as 200 °C (Ringwood 1969; Anderson & Sammis 1970). However, as more host rock melts, the small amount of free water becomes a lower concentration within the melt and the melting temperature rises, approaching the anhydrous melting temperature. Consequently, for the mantle to have 5 per cent or more partial melting in the presence of 0·1 per cent water, the temperatures must be very near the anhydrous solidus (Ringwood 1969). Ringwood (1969), Green (1970), Green & Ringwood (1970) and Lambert & Wyllie (1970) suggest that the water can be supplied from the source rock by amphibole as hornblende or perhaps phlogopite. Hornblende is not stable above 1000–1100 °C (Yoder & Tilley 1962; Lambert & Wyllie 1970; Green & Ringwood 1970) and on decomposition will release water to the melt phase. In the source pyrolite, at pressures greater than about 27 kbar (Green & Ringwood 1970), hornblende will not be present and the possibilities for free water from the host rock would cease. In the models of this study the hydrostatic pressure is 27 kbar near a depth of 85 km. Therefore, the seismic discontinuities at depths 70 and 80 km in models 1 and 2 and 80 km in models A1 and A2 could be an indication of the lower extreme of the amphibole and free water region rather than the pyroxene pyrolite to garnet pyrolite phase change suggested in the previous paragraph.

The above hypothesis of the presence of a small amount of water in the melted zone immediately below a thin, hot, solid lid requires a hypothesis to explain why the lid does not melt also. In fact, this contradiction can be used as an argument against water content in the mantle. However, if heat was introduced at a significant depth into the mantle within recent geologic time, the heat transport may have not yet reached to the top of the mantle. This heat could have been introduced by anomalously large motions at the friction contact between the lithosphere and the athenosphere, or it could have been introduced by a palaeosubduction zone that is an extension of the zone at the Central American Trench.

In contrast to the model of spherical melt inclusions of Birch (1969), Walsh (1969) derived equations for elastic properties of a two-phase material composed of a solid isotropic matrix with randomly oriented thin elliptical inclusions of melt. The elastic properties of the mixture are a function of the elastic properties of the two phases, the melt concentration, and the aspect ratio of the melt zones. The cube of the aspect ratio appears in the equations for the elastic properties; whereas, the melt concentration appears only to the first power. Thin elliptical melt zones along grain boundaries are a more reasonable model for partial melting than the spherical geometry. Using the Walsh (1969) theory, Anderson *et al.* (1972) have plotted seismic velocities against melt concentration for several aspect ratios for a solid olivine matrix with basalt melt. The minimum LVZ velocity of 3·601 km s^{-1} from model A1 can be achieved with an aspect ratio of 1 and 20 per cent melting (Birch's model) or aspect ratios and per cent melting ratios, respectively, of about 5×10^{-2} and 10 per cent or 5×10^{-3} and 1 per cent. With elliptical melt zones 200 times as long as they are high, the LVZ of the four models can be interpreted as resulting from less than 10 per cent melting. Exact estimates of partial melting must wait for experimental evidence on the geometry of melt inclusions at mantle pressures and temperatures. Spetzler & Anderson (1968) have observed seismic velocities and attenuation in a NaCl, brine, ice system that showed a sudden decrease in velocity and increase in attenuation for minute concentrations of melt at the eutectic temperature. These sudden changes are in agreement with the Walsh theory.

Another factor that could create the asymmetric concentration of low velocities immediately below the lid as indicated by the inversion models 1 and A1 is the upward migration of both free water and low melting temperature minerals. In other words, this velocity structure is the consequence of differentiation of basaltic magma within the mantle. Ringwood (1969) estimates that 5 per cent partial melting is about the lower bound for the melt to become unstable and to rise forming magma chambers. Since Mexico does have current volcanic activity, the active generation of magma in the mantle is a realistic possibility.

At this point, a new hypothesis is presented on the uplift of high flat plateaus. As melting occurs, the density and the viscosity decrease and the molten material becomes more mobile and rises. When it reaches the bottom of the solid lid, it is blocked from further upward migration within the material. As melting increases, the gravity differential increases and a large uniform upward force is exerted throughout the region. Woollard (1972) gives the Bouguer gravity anomaly in the central Mexico highlands as an almost constant -200 mgal with a few small contours of -220 mgal. The Pratt–Hayford isostatic anomaly is about -20 mgal for a compensation depth of 113·7 km. These gravity anomalies substantiate the existence of a large vertical regional force. This large force acts to raise the region as a flat entity and the high plateau is formed. This hypothesis can be applied to the central highlands of Mexico by the seismic low velocities found in this study. It is possible that similar forces have created the Colorado Plateau. Very few heat flow determinations have been made in this province (Roy, Blackwell & Decker 1972). However, the Sn velocity across the Colorado Plateau from Rangely, Colorado, to QC–AZ is about 10 per cent slower than the Sn velocity from the Nevada Test Site (NTS) to QC–AZ (Fix & Sherwin 1972). This significantly slower shear-wave velocity suggests that the Colorado Plateau may have a mantle similar to central Mexico. Woollard (1972) shows a Bouguer gravity anomaly of about -200 to -280 mgal in the Colorado Plateau that is very similar to the Bouguer anomaly of -200 to -220 mgal in the central Mexico highlands. The physical processes causing the Colorado Plateau to rise may also be contributing to the east–west tensional forces within the Basin and Range Province to the west.

A low-velocity zone begins at a depth of 300 km and extends to the bottom of the models A1 and A2 at a depth of 380 km. This LVZ corresponds to similar LVZ's in the shear-wave models of Ibrahim & Nuttli (1967) and Hales & Roberts (1970). Two possible mechanisms could cause the LVZ at these depths. This depth is the region of the transition from olivine to spinel. Spinel has a low critical thermal gradient for shear-wave velocity. For a temperature gradient greater than 0·69 °C km^{-1} in spinel the shear-wave velocity will decrease with depth (Liebermann & Schreiber 1969; Anderson & Sammis 1970). The second possible mechanism is the decrease of the shear modulus from instability in the crystal lattices prior to the olivine–spinel solid–solid phase change (Anderson & Julian 1969; Ahrens 1972). The extreme low velocities of models A1 and A2 and the high temperature gradients in the upper mantle, suggest that both mechanisms are probably in effect in central Mexico.

The central Mexico geotherm is plotted in Fig. 22 on a diagram of the pressure and temperature fields for crustal rocks. The solidus curve for water saturated granite and the solidus and liquidus curve for water saturated olivine tholeiite in Fig. 22 are taken from Yoder & Tilley (1962). The depths for model FBR3 are given at the corresponding hydrostatic pressures and the low-velocity regions of models 1 and 2 are indicated. The olivine tholeiite was selected as a typical basalt, but other basaltic compositions have similar solidus and liquidus curves (Yoder & Tilley 1962). The central Mexico geotherm intersects the basalt solidus exactly at the beginning of the LVZ. These data imply that the base of the crust very probably is a partially molten zone. Anderson & Sammis (1970) reached the similar conclusion that in the Basin and Range province partial melting is implied at the base of the crust. Accord-

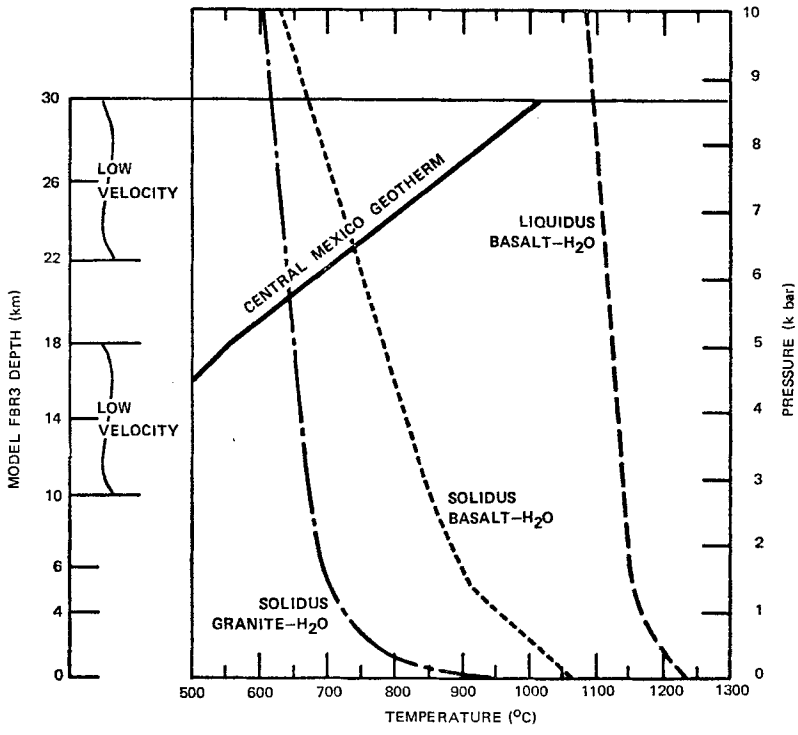

FIG. 22. Central Mexico geotherm model diagrammed with pressure and temperature curves for water saturated granite and olivine tholeiite after Yoder & Tilley (1962).

ing to the thermal models in Tables 9 and 10 the temperatures at the 30 km depth in central Mexico are about 220 °C higher than in the Basin and Range. Another explanation of the LVZ in the basaltic layer is the thermal gradient of 38 °C km^{-1}. This gradient is well in excess of the 2–3 °C km^{-1} critical gradient for common minerals (Liebermann & Schreiber 1969). Thus, this LVZ can be explained only in terms of the high thermal gradient and it is not necessary to insist on a water saturated rock or even on partial melting.

The central Mexico geotherm does not hit the water saturated granite solidus until depths below the granitic layer implying that the granitic layer does not have partial melting. In the granitic layer the gradient of the geotherm is 29 °C km^{-1}. This gradient is also well in excess of the critical gradient for common minerals and explains the LVZ.

The extreme low velocities found in the inversion models are capable of explaining the large *S*-wave station residuals. Doyle & Hales (1967) and Hales & Herrin (1972) report *S* residuals for stations within the US that range from −4·5 s (early) in the midwest to +3·3 s (late) in the Basin and Range Province. Previous shear-wave models have not provided sufficient time delays to explain this maximum 7·8 s time difference. The time for shear waves to travel vertically through several models from a 400 km depth is given in Table 11 relative to the 88·40 s required to travel through the CANSD model of Brune & Dorman (1963). The CANSD model is taken as representative of the stable pre-Cambrian shields with the fastest times of any tectonic province. From the table, it can be seen that all previous models, including the several that were based only on seismic waves that traversed the Basin and Range province,

Table 11

Shear-wave travel times from a depth of 400 *km to the surface for several models*

Model	Time through model minus time through model CANSD (sec)	Reference
CANSD	0*	Brune & Dorman (1963)
DUG–TUC	0·22	Wickens & Pec (1968)
Lehman (NE America)	0·43	Dorman *et al.* (1960)
STAN 3 (TFO array)	1·16	Kovach & Robinson (1969)
Ibrahim & Nuttli (US and NTS)	1·29	Ibrahim & Nuttli (1967) Nuttli (1969)
SLUTD1 (US)	1·44	Hales & Roberts (1970)
FBR3A (Basin and Range)	2·54	This study
B & R III	4·60	Pilant (1967)
Model A1	7·46	This study
Model A2	7·59	This study
Model 1	8·14	This study
Model 2	12·28	This study

* Absolute time through CANSD is 88·40 s

cannot explain the 7·8-s travel-time difference. Models A1 and A2 of this study provide 7·46 and 7·59 s delays and almost exactly explain the variations in station residuals that have been observed. Model 1 exceeds the travel time slightly, but model 2 is too slow. These times are the result of the low velocities at depths below 120 km in models 1 and 2 that are unrealistic and that are below the depth of accurate velocities for the high resolution model. The models from this study can explain the *S*-wave station residuals because the path through central Mexico has the low velocity structure over a sufficient distance that it can be accurately sampled with surface waves. The areas in the Basin and Range Province with the highest *S*-wave station residuals are smaller. Unless carefully planned, surface-wave studies in these areas will average the regions of lowest velocities with regions of higher velocities to obtain intermediate models that cannot explain the *S*-wave residuals. Refraction *P*-wave studies have a similar sampling problem and the lowest velocities are averaged with higher velocities along the path. Inversion of body wave travel time and $dT/d\Delta$ curves does not provide a unique solution (Gerver & Markushevich 1966; Wiggins, McMechan & Toksöz 1973) in the low velocity zone and investigators to date have not found it necessary to try models with low velocities as extensive as found in this surface-wave study.

Summary

Group velocity dispersion curves have been determined by multiple filter analysis for a path across central Mexico for the fundamental mode, first higher mode, and second higher mode for Rayleigh waves and for Love waves. The fundamental mode curves have slower velocities than average continental paths. Both the Rayleigh-wave and the Love-wave curves peak at a period of about 60 s and decrease toward longer periods.

Eighteen closely-grouped earthquakes and ultra-high-sensitivity three-component

inertial LP seismographs and three-component strain LP seismographs provided 108 earthquake-instrument pairs. This quantity of data provided a basis for investigating errors in group velocity determinations. The average deviation from the mean was between about 0·025 and 0·060 km s^{-1} for Rayleigh waves and Love waves at periods shorter than 35 s. At longer periods the average deviation was between about 0·060 and 0·160 km s^{-1} for Rayleigh waves and between about 0·060 and 0·281 km s^{-1} for Love waves.

The inversion technique of Bloch has been extended so that many options can be exercised in the inversion program. An important addition has been a layer-iteration weighting that provides stability for the first layers encountered in a solution.

The central Mexico group velocity dispersion curves have been inverted with a least squares layer by layer technique. Two high resolution models and two more stable inversion models are presented.

These models contribute valuable insight into the composition and thermal state of the crust and mantle. All four inversion models have a 30 km thick crust with four layers: a low-velocity sedimentary layer, a sedimentary rock layer, a granitic layer with a low velocity zone resulting from a high geothermal gradient but without melting, and a basaltic layer with a low velocity zone at depths between 22 and 30 km resulting from either the high geothermal gradient or partial melting of a wet basalt or a combination of these two factors. The mantle has a thin lid that is 4–8 km thick and may have a higher than normal mantle shear-velocity. Partial melting occurs immediately below the lid. The velocities correspond to partial melting of 20 per cent according to Birch's (1969) theory of partial melting and are probably greater than 10 per cent according to Walsh's (1969) theory. The sharpness and depth of the LVZ indicate mass transport of magma to the underside of the solid lid. The low velocities and their change of partial melt with depth can be explained by an anhydrous Pyrolite III model. However, the data also suggest the need for partial water pressure in the mantle. The water comes from amphiboles that do not remain stable at pressures corresponding to a depth of about 70 km. The sharp velocity increase at this depth is possibly a combination of the bottom of the water zone and phase change from pyroxene pyrolite to olivine pyrolite. The partial melt zone continues to a depth of 260 km in the anhydrous condition with smaller percentages of melt. At a depth of 300 km, another low velocity zone begins probably under the combined effect of instabilities in the crystal lattices just prior to the olivine–spinel solid–solid phase change and of the geothermal gradient exceeding the 0·69 °C km^{-1} critical shear-wave gradient of spinel. The instabilities in the crystal structure result in a negative pressure derivative for the shear modulus. Supplementary correlation is obtained for the partial melting and the low velocities by large negative Bouguer gravity anomalies and by a representative calculated geotherm and the melting temperatures of crust and mantle rock species.

The shear-wave velocities of the four inversion models are the first published that can explain the 7·8-s *S* station residual variation in North America.

A new hypothesis is presented concerning high flat plateaus. As melting occurs, density decreases providing a buoyancy force and viscosity decreases aiding mobility of the molten mass. The melting and mobility are aided by partial water pressure available from melted amphiboles. The light hot magma rises to the base of the lid where further movement is blocked. However, the ligher material exerts a regionally uniform vertical force that is capable of lifting the central Mexico highlands normal to the local gravity vector. It is suggested that the Colorado Plateau may be the result of a similar regional uplift.

Acknowledgments

The operation of the Queen Creek Seismological Station was supported by the

Advanced Research Projects Agency, Nuclear Test Detection Office, under Project VELA-UNIFORM and accomplished under the technical direction of the Air Force Technical Applications Center under Contract F33657-69-C-0121. The research reported in this paper was accomplished independently by the author with assistance provided by Teledyne Geotech for computer time and preparation of the typescript and illustrations. The author thanks Professor Anton L. Hales for advice and encouragement during the full course of this effort. He also thanks his many colleagues for their support and assistance.

12433 *Coventry Road*,
Dallas, Texas 75230,
USA

References

Ahrens, T. J., 1972. The state of mantle minerals, in *The upper mantle, Tectonophysics*, ed. A. R. Ritsema, **13,** 189–219.

Alterman, Z., Jarosch, H. & Pekeris, C. L., 1961. Propagation of Rayleigh waves in the earth, *Geophys. J. R. astr. Soc.*, **4,** 219–241.

Anderson, D. L. & Julian, B. R., 1969. Shear velocities and elastic parameters of the mantle, *J. geophys. Res.*, **74,** 3281–3286.

Anderson, D. L. & Sammis, C., 1970. Partial melting in the upper mantle, *Phys. Earth Planet. Int.*, **3,** 41–50.

Anderson, D. L., Sammis, C. & Jordan, T., 1972. Composition of the mantle and core, in *The nature of the solid earth*, 41–66, ed. E. C. Robertson, McGraw–Hill Inc., New York.

Archambeau, C. B., Flinn, E. A. & Lambert, D. G., 1969. Fine structure of the upper mantle, *J. geophys. Res.*, **74,** 5825–5865.

Backus, G., 1970a. Inference from inadequate and inaccurate data, I, *Proc. Nat'l. Acad. Sci.*, **65,** 1–7.

Backus, G., 1970b. Inference from inadequate and inaccurate data, II, *Proc. Nat'l. Acad. Sci.*, **65,** 281–287.

Backus, G., 1970c. Inference from inadequate and inaccurate data, III, *Proc. Nat'l. Acad. Sci.*, **67,** 282–289.

Backus, G. E. & Gilbert, J. F., 1967. Numerical applications of a formalism for geophysical inverse problems, *Geophys. J. R. astr. Soc.*, **13,** 247–276.

Backus, G. & Gilbert, F., 1968. The resolving power of gross earth data, *Geophys. J. R. astr. Soc.*, **16,** 169–205.

Backus, G. & Gilbert, F., 1970. Uniqueness in the inversion of inaccurate gross earth data, *Phil. Trans. R. Soc. London, Ser. A.*, **266,** 123–192.

Birch, F., 1969. Density and composition of the upper mantle: first approximation as an olivine layer, in *The Earth's crust and upper mantle, Geophysical Monograph* 13; American Geophysical Union, Washington, 18–36.

Birch, F., Roy, R. F. & Decker, E. R., 1968. Heat flow and thermal history in New England and New York, in *Studies of Appalacian Geology: Northern and Maritime*, 437–451, eds E-an Zen, W. S. White, J. B. Hadley & J. F. Thompson, Interscience, New York.

Biswas, N. N. & Knopoff, L., 1970. Exact earth-flattening calculations for Love waves, *Bull. seism. Soc. Am.*, **60,** 1123–1137.

Blackwell, D. D., 1971. The thermal structure of the continental crust, in *The structure and physical properties of the earth's crust, Monograph* 14, 169–184, ed. J. G. Heacock, Amer. Geophys. Union, Washington.

Bloch, S., 1969. *Surface wave dispersion in Southern Africa*, PhD Thesis, University of Witwatersrand, 148 p.

Bloch, S., Hales, A. L. & Landisman, M., 1969. Velocities in the crust and upper mantle of southern Africa from multi-mode surface wave dispersion, *Bull. seism. Soc. Am.*, **59**, 1599–1679.

Boore, D. M. & Toksöz, M. Nafi, 1969. Rayleigh wave particle motion and crustal structure, *Bull. seism. Soc. Am.*, **59**, 331–346.

Bracewell, R., 1965. *The Fourier transform and its applications*, McGraw–Hill Book Co., New York, 381 pp.

Brune, J. & Dorman, J., 1963. Seismic waves and earth structure in the Canadian Shield, *Bull. seism. Soc. Am.*, **53**, 167–210.

Claerbout, J. F. & Muir, F., 1973. Robust modeling with erratic data, *Geophysics*, **38**, 826–844.

Clark, S. P., ed., 1966. *Handbook of physical constants, Memoir* 97: The Geological Soc. Am., New York, 587 p.

Clark, S. P. & Ringwood, A. E., 1964. Density distribution and constitution of the mantle, *Rev. Geophys.*, **2**, 35–88.

Cserna, Z. de, 1961. *Tectonic map of Mexico*, Geological Society of America.

Der, Z., Massé, R. & Landisman, M., 1970. Effects of observational errors on the resolution of surface waves at intermediate distances, *J. geophys. Res.*, **75**, 3399–3409.

Der, Z. A. & Landisman, M., 1972. Theory for errors, resolution and separation of unknown variables in inverse problems, with application to the mantle and the crust in Southern Africa and Scandinavia, *Geophys. J. R. astr. Soc.*, **27**, 137–178.

Dorman, J. & Ewing, M., 1962. Numerical inversion of seismic surface wave dispersion data and crust-mantle structure in New York–Pennsylvania area, *J. geophys. Res.*, **67**, 5227–5241.

Dorman, J., Ewing, M. & Oliver, J., 1960. Study of shear-velocity distribution in the upper mantle by mantle Rayleigh waves, *Bull. seism. Soc. Am.*, **50**, 87–115.

Doyle, H. A. & Hales, A. L., 1967. An analysis of the travel times of *S* waves to North American Stations, in the distance range 28° to 82°, *Bull. seism. Soc. Am.*, **57**, 761–771.

Dziewonski, A., Bloch, S. & Landisman, M., 1969. A technique for the analysis of transient seismic signals, *Bull. seism. Soc. Am.*, **59**, 427–444.

Dunkin, J. W., 1965. Computation of modal solutions in layered, elastic media at high frequencies, *Bull. seism. Soc. Am.*, **55**, 335–358.

Fix, J. E. & Sherwin, J. R., 1970. A high-sensitivity strain/inertial seismograph installation, *Bull. seism. Soc. Am.*, **60**, 1803–1822.

Fix, J. E. & Sherwin, J. R., 1972. *Development of LP wave discrimination capability using LP strain instruments, Final Report, Project VT/8706, Technical report no.* 72–3: Teledyne Geotech, Garland, 597 pp.

Freedman, H. W., 1966. A statistical discussion of P_n residuals from explosions, *Bull. seism. Soc. Am.*, **56**, 677–695.

Freedman, H. W., 1968. Seismological measurements and measurement error, *Bull. seism. Soc. Am.*, **58**, 1261–1271.

Gerver, M. & Markushevich, V., 1966. Determination of seismic wave velocity from the travel-time curve, *Geophys. J. R. astr. Soc.*, **11**, 165–173.

Green, D. H., 1970. A review of experimental evidence on the origin of basaltic and nephelinitic magmas, *Phys. Earth Planet. Int.*, **3**, 221–235.

Green, D. H. & Ringwood, A. E., 1970. Mineralogy of peridotitic compositions under upper mantle conditions, *Phys. Earth Planet. Int.*, **3**, 359–371.

Green, R. W. E. & Hales, A. L., 1968. The travel times of *P* waves to 30° in the central United States and upper mantle structure, *Bull. seism. Soc. Am.*, **58**, 267–289.

Hales, A. L. & Herrin, E., 1972. Travel times of seismic waves, in *The nature of the solid earth*, 172–215, ed. E. C. Robertson, McGraw–Hill Inc , New York.

Hales, A. L. & Roberts, J. L., 1970. Shear velocities in the lower mantle and the radius of the core, *Bull. seism. Soc. Am.*, **60**, 1427–1436.

Harkrider, D. G., 1964. Surface waves in multi-layered elastic media, 1. Rayleigh and Love-waves from buried sources in a multi-layered elastic half-space, *Bull. seism. Soc. Am.*, **54**, 627–697.

Harkrider, D. G., 1968. The perturbation of Love-wave spectra, *Bull. seism. Soc. Am.*, **58**, 861–880.

Haskell, N. A., 1953. Dispersion of surface waves on multi-layered media, *Bull. seism. Soc. Am.*, **43**, 17–34.

Herrin, E., 1972. A comparative study of upper mantle models: Canadian Shield and Basin and Range Provinces, in *The nature of the solid earth*, 216–231, ed. E. C. Robertson, McGraw–Hill Inc., New York.

Herrmann, R. B., 1973. Some aspects of band-pass filtering of surface waves, *Bull. seism. Soc. Am.*, **63**, 663–671.

Ibrahim, A.-B. & Nuttli, O. W., 1967. Travel-time curves and upper-mantle structure from long-period *S* waves, *Bull. seism. Soc. Am.*, **57**, 1063–1092.

Jackson, D. D., 1972. Interpretation of inaccurate, insufficient and inconsistent data, *Geophys. J. R. astr. Soc.*, **28**, 97–109.

James, D. E., 1971a. Anomalous Love-wave phase velocities, *J. geophys. Res.*, **76**, 2077–2083.

James, D. E., 1971b. Andean crustal and upper mantle structure, *J. geophys. Res.*, **76**, 3246–3271.

Johnson, L. R., 1967. Array measurements of *P* velocities in the upper mantle, *J. geophys. Res.*, **72**, 6309–6325.

King, P. B., Compiler, 1969. *Tectonic map of North America*, United States Geological Survey.

Knopoff, L., 1972. Observation and inversion of surface-wave dispersion, in *The upper mantle, Tectonophysics*, ed. A. R. Ritsema, **13**, 497–519.

Knopoff, L. & Schwab, F. A., 1968. Apparent initial phase of a source of Rayleigh waves, *J. geophys. Res.*, **73**, 755–760.

Kovach, R. L. & Robinson, R., 1969. Upper mantle structure in the Basin and Range Province, western North America, from apparent velocities of *S* waves, *Bull. seism. Soc. Am.*, **59**, 1653–1665.

Lambert, J. B. & Wyllie, P. J., 1970. Melting in the deep crust and upper mantle and the nature of the low velocity layer, *Phys. Earth Planet. Int.*, **3**, 316–322.

Lanczos, C., 1956. *Applied analysis*, Prentice Hall, Englewood Cliffs, 539 pp.

Lehmann, I., 1955. The times of *P* and *S* in northeastern America, *Ann. di Geofisica*, **8**, 351–370.

Liebermann, R. C. & Schreiber, E., 1969. Critical thermal gradients in the mantle, *Earth Planet. Science Letts*, **7**, 77–81.

Massé, R. P., 1971. *Seismic studies of the Earth's mantle*, PhD Thesis, Southern Methodist University.

Massé, R. P., Landisman, M. & Jenkins, J. B., 1972. An investigation of the upper mantle compressional velocity distribution beneath the Basin and Range Province, *Geophys. J. R. astr. Soc.*, **30**, 19–36.

McEvilly, T. V., 1964. Central U.S. crust-upper mantle structure from Love and Rayleigh wave phase velocity inversion, *Bull. seism. Soc. Am.*, **54**, 1997–2015

Nuttli, O. W., 1969. Travel times and amplitudes of *S* waves from nuclear explosions in Nevada, *Bull. seism. Soc. Am.*, **59**, 385–398.

Papazachos, B. C., 1964. Dispersion of Rayleigh waves in the Gulf of Mexico and Caribbean Sea, *Bull. seism. Soc. Am.*, **54**, 909–925.

Papoulis, A., 1962. *The Fourier integral and its applications*, McGraw–Hill Book Co., New York, 318 pp.

Parker, R. L., 1972. Inverse theory with grossly inadequate data, *Geophys. J. R. astr. Soc.*, **29**, 123–138.

Pilant, W. L., 1967. *Final technical report, Tectonic features of the earth's crust and upper mantle*, University of Pittsburgh, Pittsburgh, 43 p. (Clearinghouse for Federal Scientific and Technical Information Document AD-658053).

Pilant, W. L. & Knopoff, L., 1970. Inversion of phase and group slowness dispersion, *J. geophys. Res.*, **75**, 2135–2136.

Press, F., 1966. Seismic velocities, in *Handbook of physical constants, Memoir* 97, 196–218, ed. S. P. Clark, The Geological Soc., Am., New York.

Ringwood, A. E., 1969. Composition and evolution of the upper mantle, in *The earth's crust and upper mantle, monograph* 13, 1–17, ed. P. J. Hart, Amer. Geophys. Union, Washington.

Roy, R. F., Blackwell, D. D. & Decker, E. R., 1972. Continental heat flow, in *The nature of the solid earth*, 506–543, ed. E. C. Robertson, McGraw–Hill Inc., New York.

Santo, T., 1965. Lateral variation of Rayleigh-wave dispersion character, Part II; Eurasia, *Pure Appl. Geophys.*, **62**, 67–80.

Satô, Y., Usami, T. & Landisman, M., 1968. Theoretical seismograms of torsional disturbances excited at a focus within a heterogeneous spherical earth-case of a Gutenberg–Bullen A′ earth model, *Bull. seism. Soc. Am.*, **58**, 133–170.

Spetzler, H. & Anderson, D. L., 1968. The effect of temperature and partial melting on velocity and attenuation in a simple binary system, *J. geophys. Res.*, **73**, 6051–6060.

Steinhart, J. S. & Meyer, R. P., 1961. *Explosion studies of continental structure, Publ.* 622, Carnegie Institute of Washington, Washington, 409 pp.

Talwani, M., Sutton, G. H. & Worzel, J. L., 1959. A crustal section across the Puerto Rico Trench, *J. geophys. Res.*, **64**, 1545–1555.

Tarr, A. C., 1969. Rayleigh-wave dispersion in the North Atlantic Ocean, Caribbean Sea and Gulf of Mexico, *J. geophys. Res.*, **74**, 1591–1607.

Thatcher, W. & Brune, J. N., 1973. Surface waves and crustal structure in the Gulf of California region, *Bull. seism. Soc. Am.*, **63**, 1689–1698.

Thompson, W. T., 1950. Transmission of elastic waves through a stratified solid medium, *J. appl. Phys.*, **21**, 89–93.

Tolstoy, I. & Usdin, E., 1953. Dispersive properties of stratified elastic and liquid media: a ray theory, *Geophysics*, **18**, 844–870.

Tucker, W., Herrin, E. & Freedman, Helen W., 1968. Some statistical aspects of the estimation of seismic travel times, *Bull. seism. Soc. Am.*, **58**, 1243–1260.

Walsh, J. B., 1969. New analysis of attenuation in partially melted rock, *J. geophys. Res.*, **74**, 4333–4337.

Warren, D. H., 1969. A seismic refraction survey of crustal structure in central Arizona, *Bull. geol. Soc. Am.*, **80**, 257–282.

Wickens, A. J. & Pec, K., 1968. A crust-mantle profile from Mould Bay, Canada to Tucson, Arizona, *Bull. seism. Soc. Am.*, **58**, 1821–1831.

Wiggins, R. A. & Helmberger, D. V., 1973. Upper mantle structure of the western United States, *J. geophys. Res.*, **78**, 1870–1880.

Wiggins, R. A., McMechan, G. A. & Toksöz, M. N., 1973. Range of earth structure nonuniqueness implied by body wave observations, *Rev. Geophys. Space Phys.*, **11**, 87–113.

Woollard, G. P., 1972. Regional variations in gravity, in *The nature of the solid earth*, 463–505, ed. E. C. Robertson, McGraw–Hill Inc., New York.

Yoder, H. S. & Tilley, C. E., 1962. Origin of basalt magmas: an experimental study of natural and synthetic rock systems, *J. Petrol.*, **3**, 342–532.